

Modeling Friction through the use of a Genetic Algorithm

by

Marek Andrzej Krzeminski

A thesis

presented to the University of Waterloo

in fulfillment of the

thesis requirement for the degree of

Master of Applied Science

in

Electrical and Computer Engineering

Waterloo, Ontario, Canada, 2003

©Marek Andrzej Krzeminski, 2003

I hereby declare that I am the sole author of this thesis.

I authorize the University of Waterloo to lend this thesis to other institutions or individuals for the purpose of scholarly research.

Marek Andrzej Krzeminski

I further authorize the University of Waterloo to reproduce this thesis by photocopying or by other means, in total or in part, at the request of other institutions or individuals for the purpose of scholarly research.

Marek Andrzej Krzeminski

Borrower's Page

The University of Waterloo requires the signatures of all persons using or photocopying this thesis. Please sign below, and give address and date.

A c k n o w l e d g e m e n t s

I would like to give extra special thanks to Dr. David Wang for taking me on as one of his graduate students, and helping me through the two years of work that I put into this thesis.

I would also like to thank Mona El-Tahan, Wenfang Xie and Hussein El-Tahan from InCoreTec Incorporated for presenting me with the opportunity to work on this project. It was many hours of work, but very rewarding in the end. A thanks also goes out to Yves Gonthier from the Canadian Space Agency for pointing me in the right direction during my time in need.

Special thanks also goes out to Dr. Eric Kubica, Kevin Krauel and Derek Wight for giving me inspiration and new ideas to help me continue to pursue my research.

The support I received from Dave's wonderful grad students was a great benefit, and it helped me to finish my thesis. So everyone deserves a pat on the back. Thanks Stanley Fok, Kingsley Fregene, Gilbert Lai, Kevin Leung, Grace Ni, Thambirajah Ravichandran, Joseph Shu, Craig Turner and Kamyar Ziaei (I hope I haven't missed anyone!).

Finally I would like to thank my readers, Dr. Glenn Heppler, Dr. Kevin Tuer, and Dr. David Wang for taking the time to read my thesis during the holiday season.

A b s t r a c t

In the field of robotics, joint friction is an impediment that can have significant negative impact on robot performance by limiting positional accuracy, causing loss of energy and potential instability in applications such as force control and tele-operation. The purpose of this thesis is to discuss a robust friction compensation technique that has been developed for an electric motor, which is an integral part of many industrial robots.

This friction compensation modeling technique combines the structure of a mathematical friction model with the optimization capabilities of a Genetic Algorithm. The best combined friction model and motor model (identified by using the Genetic Algorithm off-line) that fits experimentally collected data is used to implement a model-based friction compensator. The addition of the model-based friction compensator into a system results in that system behaving as if it were nearly linear. The friction compensated system also allows for the design of a LTI compensator in the feed-forward path to further improve the performance of the overall system. Extensive experimental testing on a harmonic drive confirms that this technique, causes the compensated system to behave almost like an ideal linear system without friction.

Table of Contents

Borrower's Page.....	iii
Acknowledgements.....	iv
Abstract.....	v
Table of Contents.....	vi
List of Figures.....	viii
List of Tables.....	ix
Chapter 1 Introduction.....	1
Chapter 2 Background.....	4
2.1 Friction Phenomena.....	4
2.2 Friction Modeling Considerations.....	6
2.2.1 Dry vs. Lubricated.....	6
2.2.2 Friction Regimes.....	6
2.2.3 Compensation Tasks.....	8
2.2.4 Static Friction and Break-Away Force.....	9
2.2.5 Friction Lag.....	11
2.2.6 Stribeck Effect.....	11
2.2.7 Directional and Position Effects.....	12
2.2.8 Rolling vs. Sliding Friction.....	12
2.2.9 Time Dependence.....	12
2.3 Friction Models.....	12
2.3.1 Classical Models.....	13
2.3.2 Choices for $F(v)$	16
2.4 Friction Model Summary.....	21
Chapter 3 Friction Model Parameter Identification Using a Genetic Algorithm.....	23
3.1 Genetic Algorithm.....	23
3.2 Structure of a Genetic Algorithm.....	24
3.2.1 Genetic Algorithm Example.....	27
3.3 Using a GA to do Friction Modeling.....	30

3.3.1 Evaluation Criterion.....	30
3.4 Summary.....	33
Chapter 4 Genetic Algorithm Details.....	34
4.1 Sequence of GA Operations	34
4.1.1 Collecting Real Input & Output Data Pair	34
4.1.2 Motor Model Structure	37
4.1.3 Friction Model Structures.....	37
4.1.4 Setting other GA Parameters.....	43
4.1.5 Running the GA	45
4.1.6 Analyzing results from the GA.....	50
4.2 Genetic Algorithm Summary	51
Chapter 5 How To Use The GA Results.....	52
5.1 Friction Compensation Methodology.....	52
5.2 Limitation of the Friction Compensator	54
5.3 Experimental Results.....	55
5.4 Applied Friction Compensation Summary	64
Chapter 6 Conclusions and Recommendations.....	65
Glossary	68
Appendix A Uniform Random Variable Theory.....	70
Appendix B Harmonic Drive Construction.....	72
Appendix C Experimental Setup Inputs.....	74
Bibliography	76

List of Figures

Figure 2.1 Friction Reaction Force	4
Figure 2.2 Friction Regimes.....	7
Figure 2.3 Relationship Between Friction and Displacement.....	10
Figure 2.4 Characteristic Relationship Between Rate.....	10
Figure 2.5 Pre-Sliding Displacement as Found by [33].....	11
Figure 2.6 Examples of Friction Models.	14
Figure 2.7 Exponential Model Curve Characteristics	17
Figure 3.1 Genetic Algorithm Flow.....	26
Figure 3.2 GA Solutions Plotted on Evaluation Curve	28
Figure 3.3 Crossover Operation.....	29
Figure 3.4 Real Data Collection Hardware Setup.....	31
Figure 3.5 Simulation Data Collection Software Setup	32
Figure 3.6 Evaluation Criterion Setup.....	33
Figure 4.1 Decreasing Amplitude Chirp Signal.....	36
Figure 4.2 Flow Chart of GA	46
Figure 4.3 Simulation Environment	47
Figure 5.1 Model of the Motor Under Test	52
Figure 5.2 Friction Compensation Setup.....	53
Figure 5.3 Experimental Setup	55
Figure 5.4 Experimental System Block Diagram.....	56
Figure 5.5 Collected Input and Output Data Pair	58
Figure 5.6 Identified Constant Velocity Friction Model	59
Figure 5.7 Experimental Setup Results	61
Figure 5.8 Second Experiment Setup Results	62
Figure 5.9 Backdrivability Results.....	64

List of Tables

Table 2.1 Summary of Friction Model characteristics	22
Table 4.1 Summary of Friction Models.....	38
Table 4.2 Exponential Friction Modeling Capabilities	39
Table 4.3 Tustin Friction Modeling Capabilities.....	40
Table 4.4 Non-Linear Friction Modeling Capabilities	41
Table 4.5 Dupont Friction Modeling Capabilities	42
Table 4.6 Seven-Parameter Friction Modeling Capabilities	43
Table 5.1 Equipment.....	56
Table 5.2 Exponential Model Parameterization.....	58
Table 5.3 Motor Model Parameterization.....	59

Chapter 1

Introduction

In the field of robotics, joint friction is an impediment that can have significant negative impact on robot performance by limiting positional accuracy, causing loss of energy and potential instability in applications such as force control and tele-operation. The purpose of this thesis is to discuss a friction compensation technique that has been developed for an electric motor, which is an integral part of many industrial robotic systems.

A friction compensated system would be of interest to many companies, especially to those whose primary industry deals with systems that require precise motion control. Medical robots (which are used for micro surgery), packaging machinery and electronic assembly robots are just a few examples of systems which would benefit from implementing a friction compensation technique.

The research performed for this thesis was motivated by the Canadian Space Agency (CSA) in the hopes that the friction compensation technique could improve the performance of harmonic drives. Harmonic drives are used by the CSA in many of their space robotic systems including the joints of the Space Station Remote Manipulator System (the International Space Station Canadarm2) and in the Special Purpose Dexterous Manipulator (SPDM), an extremely advanced, highly dexterous dual armed robot with a body, which will be used to perform delicate maintenance and servicing tasks on the International Space Station [30]. Each arm of the SPDM contains 7 joints, and each joint contains a harmonic drive to actuate motion in the arm.

The CSA, Natural Sciences and Engineering Research Council of Canada (NSERC) and InCoreTec Incorporated funded all of the research for this thesis. InCoreTec further improved the friction compensation technique presented in the thesis by adding a Neural Network into the control loop. This improved technique, dubbed the *Intelligent Friction Compensation* (IFC) technique has been filed for a provisional patent on September 24, 2002 and has been published in the proceedings of an IEEE conference [31].

In Chapter 2 of this thesis, the reader is presented with a historical background of the friction phenomenon and reasons are outlined as to why engineers would be interested in eliminating friction. To eliminate friction in a system, one must be able to model it accurately and thus the frictional effects to consider when attempting to model friction are also discussed. Chapter 2 concludes by presenting some friction model structures which have been used successfully in past experiments by other researchers.

In Chapter 3, a technique is presented that shows how all the parameter values for a friction model can be identified with the use of a Genetic Algorithm. Background information is presented on Evolutionary Algorithms and their relationship to Genetic Algorithms. An Evolutionary Algorithm is an optimization technique which is motivated by the process of natural evolution found in biological organisms.

Chapter 4 dives into the inner workings of the designed Genetic Algorithm that has been specifically created to identify friction model parameter values for the purpose of implementing a friction compensation technique. The developed Genetic Algorithm's internal sequence of events are outlined in this chapter including;

1. What input and output data pair are needed to run the Genetic Algorithm.
2. How to choose an appropriate test input.
3. Which motor model and friction model structures are used within the simulation environment.
4. What other Genetic Algorithm parameters need to be initialized for the algorithm to work properly.

Finally in Chapter 5, a procedure is shown, for a successful implementation of a friction compensator using the results gathered from the Genetic Algorithm. This friction compensation technique was used on a harmonic drive at the University of Waterloo to demonstrate that the motor exhibits improved performance when utilizing the friction compensation. The friction compensation technique was very successful since demonstrations showed that the harmonic drive exhibited improved positional accuracy when it was operated

under position control. As well, the harmonic drive was able to be backdriven, which means that an external force applied to the output shaft of the motor can cause all the mechanical transmission components, including the motors rotor to turn also. A harmonic drive is normally not backdrivable since it contains high internal friction.

Chapter 6 concludes the thesis by suggesting improvements to the developed Genetic Algorithm and directions for future research.

Chapter 2

Background

Friction is present in all mechanical systems such as bearings, transmissions, hydraulic cylinders, brakes and wheels. Friction presents itself at the physical interface between two contacting surfaces. Lubricants such as oil or grease are often used to minimize the effect of friction but it cannot be eliminated completely.

The friction phenomenon has been studied for many years in the area of tribology [1,2]. For a control engineer, friction is a very important factor when designing drive systems, high-precision servo mechanisms, robots, pneumatic and hydraulic systems. Friction is highly non-linear and may result in steady state errors, limit cycles and poor performance. Understanding how friction operates allows the control engineer to design a more reliable system which can be more accurately modeled.

2.1 Friction Phenomena

Friction is the tangential reaction force between two surfaces in contact as shown below in Figure 2.1. This reaction force is the result of many different physical effects, which depend

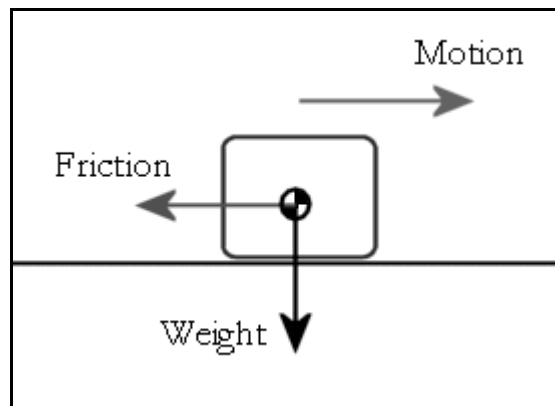


Figure 2.1 Friction Reaction Force

on contact geometry and topology, properties of the bulk and surface materials of the bodies, displacement and relative velocities of the bodies and the presence of lubrication.

In dry sliding, when two flat surfaces make contact, friction can be modeled as elastic and plastic deformation forces of microscopic asperities in contact, [3,4]. An asperity is a slight point or bump projecting out from the surface at a microscopic level.

In dry rolling contact, friction is the result of a non-symmetric pressure distribution at the contact. The pressure distribution is caused by elastic hysteresis in either of the bodies, or local sliding in the contact. For rolling friction F_f the friction coefficient, μ , is proportional to the normal load F_N [5],

$$F_f = \mu \cdot F_N. \quad (1)$$

When lubrication is added to the contacting surfaces, other physical mechanisms appear. For low velocities, the lubricant acts as a surface film, where the shear strength determines the friction. At higher velocities in low pressures, a fluid layer of lubricant is built up in the surface due to hydrodynamic effects. Friction is then determined by shear forces in the fluid layer. These shear forces depend on the viscous characteristics of the lubricant, as well as the shear velocity distribution in the fluid film. At high velocities and pressures, the lubricant layer is built up by elasto-hydrodynamic effects. In these contacts, the lubricant is transformed into an amorphous solid phase due to the high pressure. The shear forces of the solid phase turns out to be practically independent of the shear velocity [5].

The shear strength of a solid phase lubricant film at low velocities is generally higher than the shear forces of the corresponding fluid film built up at higher velocities. As a result, the friction force in lubricated systems normally decreases when the velocity increases from zero[5]. When the thickness of the film is large enough to completely separate the bodies in contact, the friction force may increase with velocity as hydrodynamic effects become significant.

Contamination is another factor that adds complications. The presence of small particles of different materials between the surfaces give rise to additional forces that strongly depend on the size and material properties of the contaminants.

The above mechanisms illustrate some of the difficulties in modeling friction. To construct a general friction model from first principles is next to impossible.

2.2 Friction Modeling Considerations

There are many details to consider when modeling friction. This section highlights some of the more dominant aspects.

2.2.1 Dry vs. Lubricated

Although there are similarities between the two scenarios, the friction dynamics of dry and lubricated surfaces can have unique features. For instance, the steady state friction force as a function of velocity for constant velocity motion between two lubricated surfaces is often described by the Stribeck curve, named after Stribeck for his work done in [6]. The dip in the frictional force at low velocities is called the Stribeck effect (see the partial fluid lubrication section of Figure 2.2). The friction-velocity relationship is application dependent and varies with material properties, temperature, wear etc.

2.2.2 Friction Regimes

Friction is complex to model because of the nature of the contact between the two sliding surfaces. The presence of asperities (peaks in the material on a microscopic level) on the material surfaces is one reason for the complexity. As the surfaces slide along one another, the peaks lock together, stretch and eventually break free. Often a lubricant is placed between the surfaces to form a boundary layer on each surface. This reduces the friction between the two surfaces since the shear strength of the boundary layer is often lower than that of the contacting materials. However, the presence of oil or grease leads to other dynamic and

velocity dependent friction effects, which can be broken down into four regimes. These regimes are shown graphically in Figure 2.2.

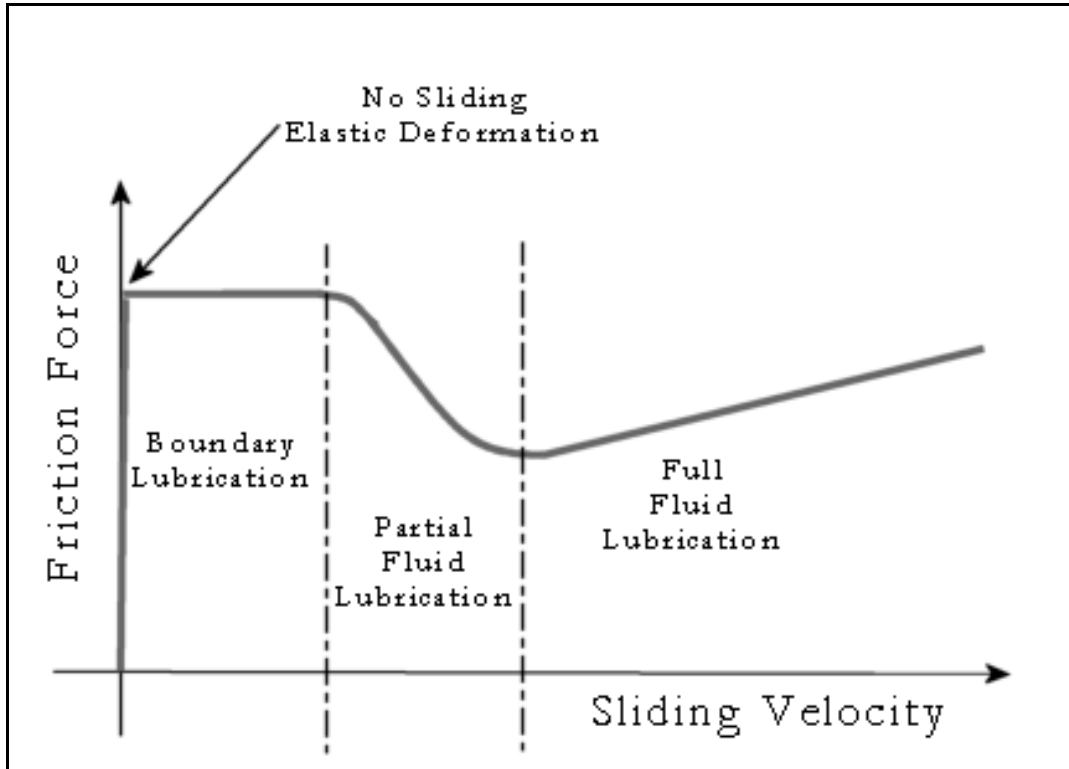


Figure 2.2 Friction Regimes

2.2.2.1 No Sliding, Elastic Deformation

In this regime, the asperities deform elastically as they make contact with one another, giving rise to microscopic motion which is often called pre-sliding displacement. This phenomenon is called the Dahl effect. Both the boundary layer and asperities deform plastically resulting in rising static friction. Eventually the spring effect between the two surfaces will reach a critical value at which point a breakaway condition occurs, allowing for true sliding. The transition from elastic contact to sliding is not simple to predict or model.

2.2.2.2 Boundary Lubrication

In this case, the relative velocity between the surfaces is small and as a result, there is still solid to solid contact. Thus, shearing occurs in the boundary lubricant. Although more the exception than the norm, the shear strength of the boundary layer can be larger than the shear strength of the solid to solid contact.

2.2.2.3 Partial Fluid Lubrication

Here, fluid is drawn into the contact region through the rolling or sliding motion of the two surfaces, thereby forming a film between them. The film is not thick enough to prevent asperitic contact though. The dynamics of partial fluid lubrication change with velocity, and as the velocity increases, the fluid layer becomes thicker. Also, as the velocity changes, there is a time lag between the instance the change in velocity occurs and the time when the steady state friction force is achieved. This is referred to as frictional lag. Due to phenomena such as these, partial fluid lubrication is often the hardest regime to model.

2.2.2.4 Full Fluid Lubrication

The last regime is characterized by the elimination of the solid to solid surface contact. Friction is generally well behaved in this regime and can generally be modeled directly proportional to the relative velocity between the moving bodies. Models that represent friction as a linear gain of velocity are said to be viscous friction models.

2.2.3 Compensation Tasks

A control engineer must gain knowledge regarding the task that the mechanism is to perform before a friction compensation technique can be designed. Reference [7] suggests four different compensation tasks.

2.2.3.1 Regulation

In this case, the mechanism is controlled to a specified set point. As a result, static friction will be a dominant friction factor. See Section 2.2.4 for a description of static friction.

2.2.3.2 Tracking and Velocity Reversals

In this case, the mechanism constantly passes through the zero velocity point. Here the mechanism may spend time at zero velocity until the force is large enough to overcome the static friction. Robots under position or force control are cited examples of mechanisms that might fall into this task category.

2.2.3.3 Tracking at Low Velocities

Here the motion is often in one direction with a constant velocity applied. During this activity stick-slip friction may dominate. Position controlled robots fall into this category.

2.2.3.4 Tracking at High Velocities

During these tasks, viscous frictional effects will dominate. Since the friction-velocity curve is positively sloped in this regime, stability is usually not an issue. High speed machinery falls into this category.

2.2.4 Static Friction and Break-Away Force

Static friction is the friction when sticking occurs. It is also commonly called stiction. The force required to overcome the stiction and initiate motion is called the break-away force. Many researchers have attempted to model this phenomenon. Rabinowicz addressed the transition between sticking and sliding in [8] where he investigated friction as a function of displacement. He concluded that the break-away force is given by the peak seen in Figure 2.3. The maximum friction force typically occurs at a small displacement from the starting point. In [9], it was found experimentally that the break-away force depends on the rate of increase

of the external force. This was confirmed in [32]. This characteristic behavior is shown in Figure 2.4.

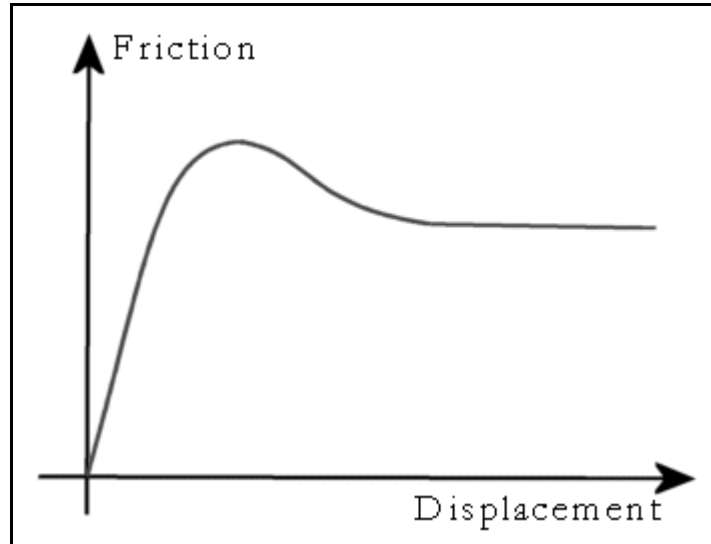


Figure 2.3 Relationship Between Friction and Displacement

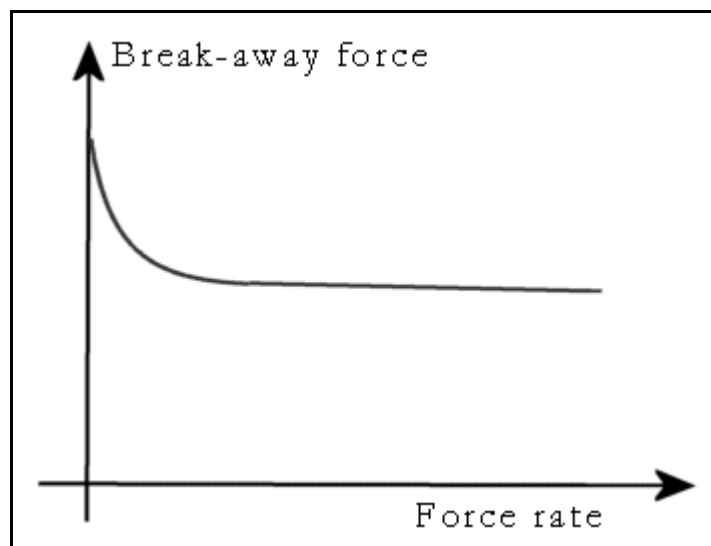


Figure 2.4 Characteristic Relationship Between Rate of Force Applied and Break-Away Force Found in [9]

Another investigation of the behavior in the sticking regime was done in [33]. Pratt and Eisner studied the spring like behavior that occurred before gross sliding. Their results were presented in diagrams showing force as a function of displacement. See Figure 2.5. The microscopic motion is often called pre-sliding motion.

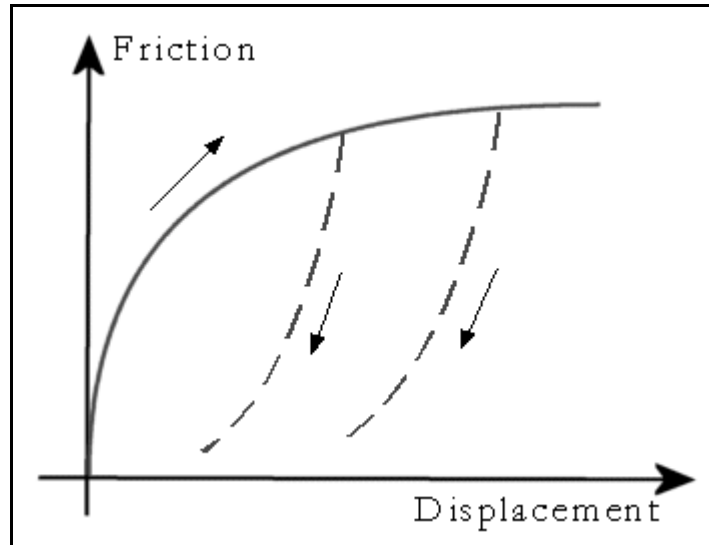


Figure 2.5 Pre-Sliding Displacement as Found by [33].
The results agree with Figure 2.3 for small displacements. Releasing the applied force results in a permanent displacement as indicated by the dashed lines.

2.2.5 Friction Lag

Frictional lag refers to the delay between a change in velocity and the corresponding change in friction. In the case of lubricated friction, this delay is reasoned to be caused by the shearing action that occurs in the lubrication boundary layer.

2.2.6 Stribeck Effect

The Stribeck phenomenon is an example of negative viscous friction. A friction model which attempts to model this effect is shown in Figure 2.6 d). As the relative velocity between two

sliding surfaces increase, the friction force decreases just after break-away. This effect has been observed experimentally in many situations and can pose significant problems such as limit cycles in control design. It has a destabilizing effect which can be offset to a certain degree by the phenomenon of frictional lag, since frictional lag causes a delay in the appearance of a destabilizing drop in friction [10].

2.2.7 Directional and Position Effects

Quite often friction will depend on the direction of the relative motion and the relative position between the two contacting surfaces. The relative position is especially predominant in gear driven systems where the meshing of the gear teeth can cause frictional anomalies.

2.2.8 Rolling vs. Sliding Friction

Pure rolling friction occurs when the contact between two surfaces is at one point. In reality, the contact area is usually larger than a point because of elasticity, thereby giving rise to a combination of pure rolling and a sliding contact. Rolling friction is a different friction process than sliding friction and should be treated as such when attempting to model friction within a mechanism.

2.2.9 Time Dependence

Another one of the more challenging tasks of friction compensation is embedding the ability to adapt to changes in the friction process caused by component wear, lubricant temperature and aging of the components. Each of these factors can influence greatly the repeatability of the friction process.

2.3 Friction Models

In this section, a summary of some friction models is presented. These models were selected from the many different models found in [34] as part of this project for the CSA. The friction

models listed below use simple equations and model friction well enough to implement a friction compensation technique over a variety of operating regimes. Each model is presented with its characteristic equation and a description is given outlining the model's operating regime.

There are many more friction models which could be used. However, these other models were found to be either simplifications of the models listed below, or they were too complex to implement for control purposes.

2.3.1 Classical Models

The classical models of friction consist of different components, which each take care of certain aspects of the friction force. The main idea is that the friction force F , opposes motion and that its magnitude is independent of velocity v and contact area. It can therefore be described as

$$F = F_C \cdot \text{sgn}(v). \quad (2)$$

Here the friction force F_C is proportional to the normal load F_N , ie $F_C = \mu F_N$ where μ is a proportionality constant. This description of friction is termed Coulomb friction (see Figure 2.6 a). Notice that the model from (2) is an ideal relay model. The Coulomb friction model does not specify the friction force for zero velocity. It may be zero or it can take on any value in the interval between $-F_C$ and F_C , depending on how the sgn function is defined. The Coulomb friction model has, because of its simplicity, often been used for friction compensation [11,12].

In the 19th century, the theory of hydrodynamics was developed leading to expressions for the friction force caused by the viscosity of lubricants [13]. The term viscous friction is used for this force component, which is usually described by (3),

$$F = \sigma \cdot v. \quad (3)$$

σ in this equation represents a proportionality constant and v is the relative velocity between the moving bodies. Viscous friction is often combined with Coulomb friction as shown in Figure 2.6 b).

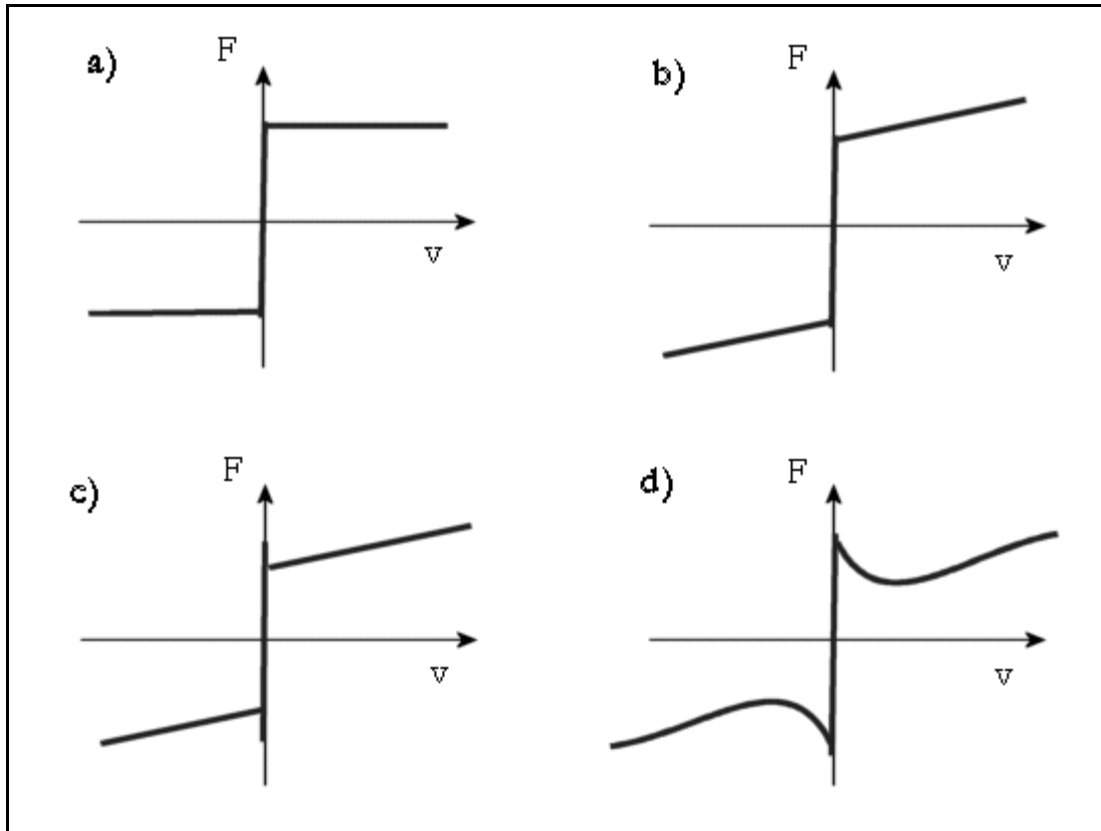


Figure 2.6 Examples of Friction Models.

Figure a) shows Coulomb friction and Figure b) Coulomb plus viscous friction. Stiction plus Coulomb and viscous friction is shown in Figure c) and Figure d) shows how the friction force may decrease continuously from the static friction level.

In [15], the idea of a friction force at rest (Static Friction) being higher than the Coulomb friction level was discussed. Static friction counteracts external forces below a certain level and thus keeps an object from moving. Friction at rest cannot be described as a function of only velocity. Instead, it has to be modeled using the external force F_e in the following way,

$$F = \begin{cases} F_e & \text{if } v = 0 \text{ and } |F_e| < F_S \\ F_S \cdot \text{sgn}(F_e) & \text{if } v = 0 \text{ and } |F_e| \geq F_S. \end{cases} \quad (4)$$

The friction force for zero velocity is a function of the external force and not the velocity. The traditional way of depicting friction in block diagrams, with velocity as the input and force as the output, is therefore not completely correct. Static friction must be expressed as a multi-valued function that can take on any value between the two extremes $-F_S$ and F_S . Specifying static friction in this way leads to the non-uniqueness of the solutions to the equations of motion for the system [15].

The classical friction components can be combined in different ways (see Figure 2.6 c), and any such combination is referred to as a classical model. These models have components that are either linear in velocity or constant.

Stribeck observed in [6] that the friction force does not decrease discontinuously as in Figure 2.6 c), but that the velocity dependence is continuous as shown in Figure 2.6 d). This is called Stribeck friction. A more general description of friction than the classical model is

$$F = \begin{cases} F(v) & \text{if } v \neq 0 \\ F_e & \text{if } v = 0 \text{ and } |F_e| < F_S \\ F_S \cdot \text{sgn}(F_e) & \text{if } v = 0 \text{ and } |F_e| \geq F_S, \end{cases} \quad (5)$$

where $F(v)$ is an arbitrary function that may look as in Figure 2.6 d). The curve is often asymmetrical.

2.3.2 Choices for $F(v)$

A number of parameterizations of $F(v)$ have been proposed and some common forms of the non-linearity are shown in the following sections. All of the friction models shown have been previously used in different systems with varying degrees of success. Each of these models have been developed to be used on a certain kind of system, and as a result, one model can not be used as a general solution for all different kinds of systems which exhibit friction.

2.3.2.1 Exponential Friction Model

Bo and Pavelescu in [16] developed a discontinuous friction model of stick slip using two exponential functions, which are based on the relative speed between two bodies, to model the acceleration and deceleration phases of the motion. This friction model takes the form,

$$F_{Exponential}(v) = \begin{cases} F_{acc} & \text{when accelerating} \\ F_{dec} & \text{when decelerating} \end{cases}$$

where

$$\begin{aligned} F_{acc} &= F_{k\min} + (F_{ST} - F_{k\min}) \cdot e^{-(\gamma \cdot v)^\delta} \\ F_{dec} &= F_{k\min} + (F_0 - F_{k\min}) \cdot e^{-(\gamma \cdot v)^\delta} \end{aligned} \quad (6)$$

F_{acc} and F_{dec} are the friction force values for the acceleration and deceleration phases respectively. $F_{k\min}$, F_{ST} , and F_0 are positive friction values that parameterize the model as shown in Figure 2.7. The relative velocity between the moving surfaces is represented by v , γ and δ are positive constants which parameterize the model. Upon expanding the exponential in a Taylor series and truncating to the second order terms, it is found that the parameter γ plays an important role in estimating the characteristics of the sliding system.

The exponential model addresses the characteristics of the stick-slip phenomena and it can predict the existence of limit cycles in a closed loop system [16].

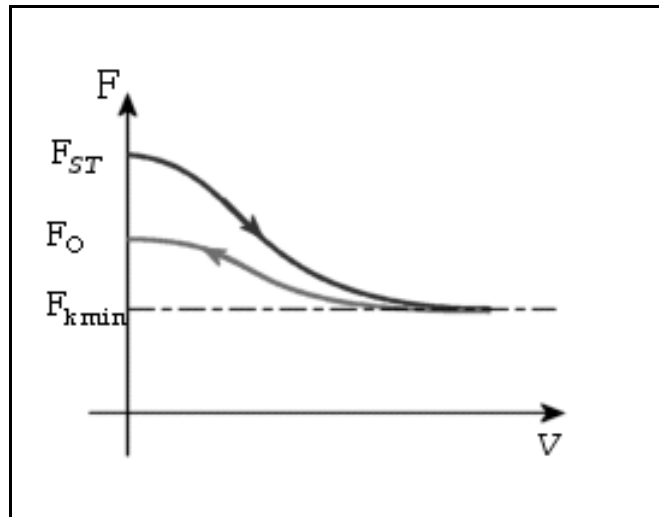


Figure 2.7 Exponential Model Curve Characteristics

2.3.2.2 Tustin Model

One of the friction models that was able to model the effects of static friction, and Coulomb friction in an experiment was credited to Tustin in [17]. His model takes the following form,

$$F_{Tustin}(v) = \left(F_{f0} - F_{fC} \cdot \left[1 - e^{\frac{-|v|}{V_c}} \right] \right) \cdot \text{sgn}(v). \quad (7)$$

$F(v)$ is the friction force, v is the velocity, F_{f0} is the static friction constant, F_{fC} is the difference between the static and dynamic friction constants, and V_c is the threshold velocity at which friction becomes dynamic. When friction becomes dynamic, this means that the friction force begins to exhibit properties that suggest that the force is strongly correlated to the relative velocity between the two contacting bodies, and possibly other phenomena.

The Tustin model used in compliance tests has illustrated the existence of the Dahl effect; however to do so, the friction parameters of this model need to vary slowly [17].

2.3.2.3 Non-Linear Friction Model

Canudas de Wit et al. proposed using a friction model in [18] which is similar to Tustin's model. It can model the effects of stiction, Coulomb and viscous friction. The model takes the form shown below,

$$F_{Non-Linear}(v) = \left[\alpha_0 + \alpha_1 \cdot e^{-\beta_1 \cdot |v|} + \alpha_2 \cdot \left(1 - e^{-\beta_2 \cdot |v|}\right) \right] \cdot \text{sgn}(v). \quad (8)$$

All five parameters in this friction model, α_0 , α_1 , α_2 , β_1 and β_2 , are positive constants. The static friction force is defined by $(\alpha_0 + \alpha_1)$, and the constant dynamic component is represented by $(\alpha_0 + \alpha_2)$ at high velocities. β_1 defines how friction decays at low velocities and β_2 defines the viscous component of friction after having reached its minimum value.

The Non-Linear friction model is used to describe the friction between an end effector and its contacting surface.

2.3.2.4 Dupont Friction Model

Another friction model developed by Dupont in [19] is shown below,

$$F_{Dupont}(v) = \left[c_0 + c_1 \cdot |v| + c_2 \cdot e^{-\left(\frac{|v|}{c_3}\right)^{c_4}} \right] \cdot \text{sgn}(v). \quad (9)$$

Here c_0 , c_1 , c_2 , c_3 , and c_4 are positive constants that parameterize the friction curve. Static friction is characterized by c_0 and viscous friction is characterized by c_1 . The threshold velocity at which friction becomes dynamic is characterized by c_3 (this is similar to V_c in the Tustin model) and c_4 estimates the characteristics of a sliding system (similar to γ in the Exponential model).

The Dupont model is able to capture the essence of frictional memory and velocity dependence. The constant velocity model was created to model both Coulomb and viscous friction effects. The model was derived by investigating the existence of frictional lag in boundary lubrication, at very low velocity regimes. One shortcoming of the model is its inability of accommodating the friction behavior at zero velocity [28].

2.3.2.5 Seven Parameter Friction Model

Many authors have focused their efforts on formulating integrated models that contain a number of components that are capable of predicting the friction force in several different regimes. It is natural to construct a model with components associated with each of the four regimes illustrated in Figure 2.2. Such is the case for the seven parameter friction model which has the following form [7],

$$F_{7\text{ parameter}}(v) = \begin{cases} F_{PS}(x) & \text{during pre-sliding} \\ F_{SL}(v, t) & \text{during sliding} \\ F_{SF}(\gamma, t_2) & \text{during static friction} \end{cases} \quad (10)$$

where

$$F_{PS}(x) = -k_t \cdot x \quad (11)$$

$$F_{SL}(v, t) = \left[F_{co} + F_{vs} \cdot |v| + F_{SF}(\gamma, t_2) \cdot \frac{1}{1 + \left(\frac{v \cdot (t - \tau_L)}{v_s} \right)^2} \right] \cdot \text{sgn}(v) \quad (12)$$

$$F_{SF}(\gamma, t_2) = F_{s,a} + (F_{s,\infty} - F_{s,a}) \cdot \frac{t_2}{t_2 + \gamma} \quad (13)$$

$F(v)$ is the instantaneous friction force, F_{co} is the Coulomb friction force constant, F_{vs} is the viscous friction force constant, F_s is the magnitude of the Stribeck friction constant, $F_{s,a}$ is the magnitude of the Stribeck friction at the end of the previous sliding period, $F_{s,\infty}$ is the magnitude of the Stribeck friction after a long time at rest, k_t is the tangential stiffness constant of the static contact, v_s is the characteristic velocity constant of the Stribeck friction, τ_L is the time constant of frictional memory, γ the positive temporal constant of the rising static friction and t_d is the dwell time (the time spent at zero velocity).

The advantage of using this model is that it is able to model all four friction regimes without discontinuities and, in simulation, the model is able to reproduce data collected for many experimental investigations. The difficulty with using the seven parameter friction model is that the switching time from one equation to the next needs to be determined in some way. Determining at which precise moment to switch equations can be difficult, and sensitive instruments may be required to identify when the system transitions from one state to the next.

2.3.2.6 LuGre Friction Model

In the past, friction was only assumed to be a function of the relative velocity between the two contacting surfaces. However, experimental observations showed that these models do not sufficiently simulate motion at very low velocities close to zero [20]. Further study resulted in the theory that motion between the two surfaces occur on a microscopic level caused by the elastic deformation of surface asperities.

Canudas de Wit et al. [20] derived a new friction model-based on the use of an internal state which treats the friction phenomena as being dynamic. This model, sometimes referred to as the LuGre model, is a state variable model formulated to model the low velocity friction using a model of the deflection of elastic bristles. This model can be broken up into two parts; a steady-state static map between velocity and friction force and dynamic friction components. The LuGre model has the form,

$$\frac{dz}{dt} = v - \frac{|v|}{g(v)} \cdot z$$

$$F = \sigma_0 z + \sigma_1 \frac{dz}{dt} + \sigma_2 v. \quad (14)$$

Here z is the state variable (the deflection of the bristles), v is the relative velocity of the contacting bodies, $g(v)$ is a function that models the constant velocity behavior, σ_0 is an equivalent stiffness for the position force relationship at velocity reversal, σ_1 is the micro-viscous friction coefficient and σ_2 is the viscous friction coefficient. The static friction model is able to capture Coulomb, Stribeck and viscous friction effects. The dynamic friction model is able to capture stick-slip motion, pre-sliding displacement, varying break-away force and frictional lag effects.

The LuGre model is able to effectively model the hysteretic effect provided that the force profile is symmetric and the motion is started from rest. There are not enough free parameters in the LuGre model to model the non-local memory aspects. As a result, the model is known to be too dissipative in pre-sliding because the model fails to account for hysteretic effects between displacement and applied force in pre-sliding [29].

The main difficulty with using the LuGre model is that the model has an extra differential equation where the z term in the model is an unmeasurable quantity. This poses a problem for the Genetic Algorithm used later because the algorithm cannot effectively converge to a friction model parameterization.

2.4 Friction Model Summary

Many different friction models have been presented in the previous sections. A summary of these models and their modeling capabilities are outlined in Table 2.1.

Table 2.1 Summary of Friction Model characteristics

	Pre-Sliding	Stick-Slip	Sliding	Stiction	Coulomb	Viscous	Varying Break-away Force
Exponential		√	√	√	√		
Tustin			√	√	√		
Non-Linear				√	√	√	
Dupont			√		√	√	
7-Parameter	√	√	√	√	√	√	√
LuGre	√	√	√*	√*	√*	√*	√
* This characteristic depends on the parameterization of the function $g(v)$							

To use any of these friction models, the values of the parameters need to be identified to validate the model for the system that is being looked at. In Chapter 3, a method using a genetic algorithm is presented to show how these friction model parameters can be identified automatically.

Chapter 3

Friction Model Parameter Identification Using a Genetic Algorithm

As seen in the previous chapter, there have been many different friction models developed over the years. Each of the models shown were developed and designed from data collected from a specific experimental setup. Each model has its own advantages and disadvantages when it comes to modeling friction, and even if two experiments that were similar in construction were used, a friction model developed for one system may not work as well on the other system due to the variations in motor characteristics and mechanical parts.

The fundamental problem lies in knowing which friction model to choose for a specific setup. Once a friction model has been chosen, the model parameter values must be found so that the friction model characterizes the system accurately. This chapter outlines a method, which uses a genetic algorithm, to find the friction model parameters for a specified friction model along with a measure of how well the model fits with experimental data. By comparing these measures for each identified friction model, the model with the best fit can be said to be the optimal friction model to use on the system that is being studied.

3.1 Genetic Algorithm

Genetic Algorithms (GA's) are a subset of a larger collection of algorithms called Evolutionary Algorithms (EA's) [42]. EA's form a class of probabilistic optimization techniques motivated by the process of natural evolution found in biological organisms. The process of evolution can be viewed as a mechanism of optimization whereby organisms are "optimized" to be better equipped to survive in a variable environment. This led to the idea that evolution, as seen in nature, could be simulated on a computer as an alternative optimization tool [22, 23, 24]. Although these algorithms are only crude simplifications of real biological processes, they have proved to be very robust. The basic idea of an EA is to evolve a population of individuals, which are potential solutions to the task at hand, over successive iterations of random variations and selection. Random variations provide the mechanism for discovering

novel solutions while selection determines which solutions are to be maintained as a basis for further exploration.

In comparison with optimization methods such as linear, quadratic, dynamic and geometric programming algorithms [25], EA's offer the following advantages which make them well suited for development of an optimization framework:

- EA's are population based search methods; therefore they can handle multi-model and/or multi-objective optimization problems.
- Due to their derivative free nature, EA's can deal with non-differential and/or non-convex objective functions effectively.
- Due to their flexible representation schemes, EA are also applicable to those optimization problems with mixed continuous-discrete design variables.
- EA and other optimization methods can be combined to form robust hybrid search methods.
- EA's provide great flexibility on incorporating problem knowledge to make an efficient implementation for a specific problem.

The price paid for the robustness that EA's offer is that EA usually require a large number of function evaluations to achieve the optimum, even for simple problems. In addition to this, there is no theoretical guarantee that an EA will always converge to the optimum solution.

3.2 Structure of a Genetic Algorithm

In a genetic algorithm, a population of individuals, which are potential solutions to the optimization problem, undergo a sequence of unary and higher order transformations (also known as mutations and crossovers respectively). These individuals strive for survival and a selection scheme, biased towards fitter individuals, selects the next generation. After a number

of generations (iterations), if the algorithm converges then the best individual or individuals represent a near-optimal solution.

Any efficient optimization algorithm must use the following two techniques to find a global optimum: *exploration* to investigate new and unknown areas in the search space, and *exploitation* to make use of the knowledge found at points previously visited to find better points in the search space. These two requirements are contradictory, and a good search algorithm must find a trade-off between the two. In EA's, this trade-off is decided mainly by two important factors; namely population diversity and selective pressure. These factors are strongly related; an increase in the selective pressure decreases the diversity of the population and vice versa. In other words, strong selective pressure supports the premature convergence of the search to a suboptimal solution and a weak selective pressure can make the search ineffective, by allowing the search to perform a random walk around the solution space.

The structure of a genetic algorithm is shown in Figure 3.1. The GA maintains a population of individuals (Parent (t)) for each generation t . Each individual represents a potential solution to the problem at hand, and is implemented as some specific data structure. Typically the initial population is generated randomly by uniformly distributing each design variable within its range of values; therefore, prior knowledge of the specific problem is desirable. The evaluation step assigns some measure of fitness to each individual based on an objective function evaluation. New individuals that may form the next generation population are created by the alteration step which performs sequences of unary and higher order transformations. Section 3.2.1 gives examples of unary and higher order transformations. The selection step forms the new population, Parent ($t + 1$) for generation $t + 1$, by selecting the most *fit* individuals from the alteration step. Each generation cycle of the GA consists of the above three steps: selection, evaluation and alteration.

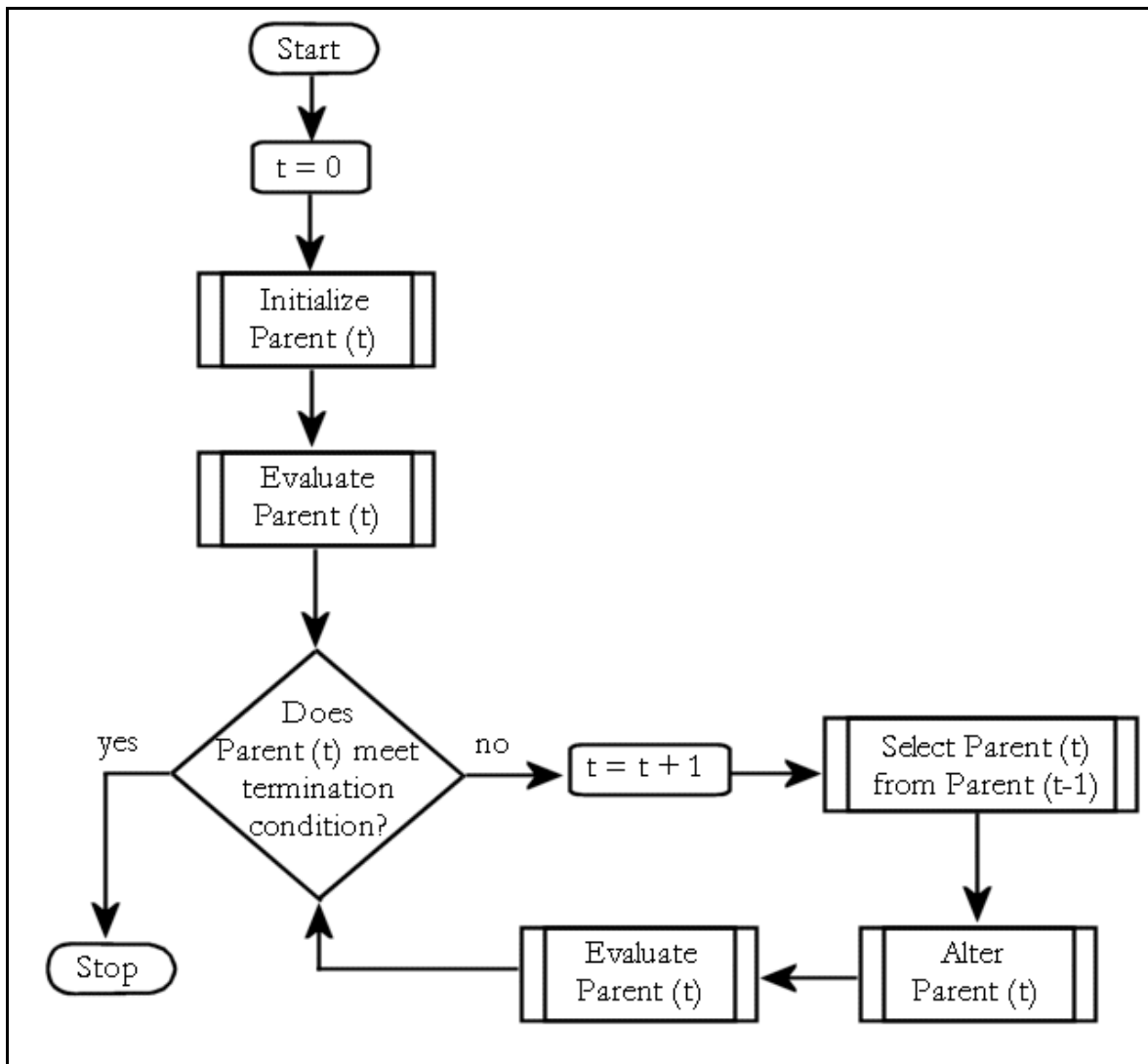


Figure 3.1 Genetic Algorithm Flow

3.2.1 Genetic Algorithm Example

To help demonstrate how a genetic algorithm works, the following simple example is presented. Suppose that the following equation is given, and the location of the maximum value is desired.

$$y = -x^2 + 3 \quad (15)$$

This equation represents a downward pointing parabola that has been shifted three units up from the origin.

The GA that will be used will select one Parent, and the alteration process will generate five new solutions (also referred to as Children) during each iteration.

Following the flow chart shown in Figure 3.1, the GA process begins by initializing. It is decided that five candidates will be generated during the initialization. For simplicity, it is also decided that the five candidates will be generated randomly by selecting values for x between $+/- 5$.

Following the initialization, the next step is evaluation. Here the randomly generated x values are evaluated in (15) to find their corresponding y values. A visual representation of the current state of the GA population could be that shown in the following figure.

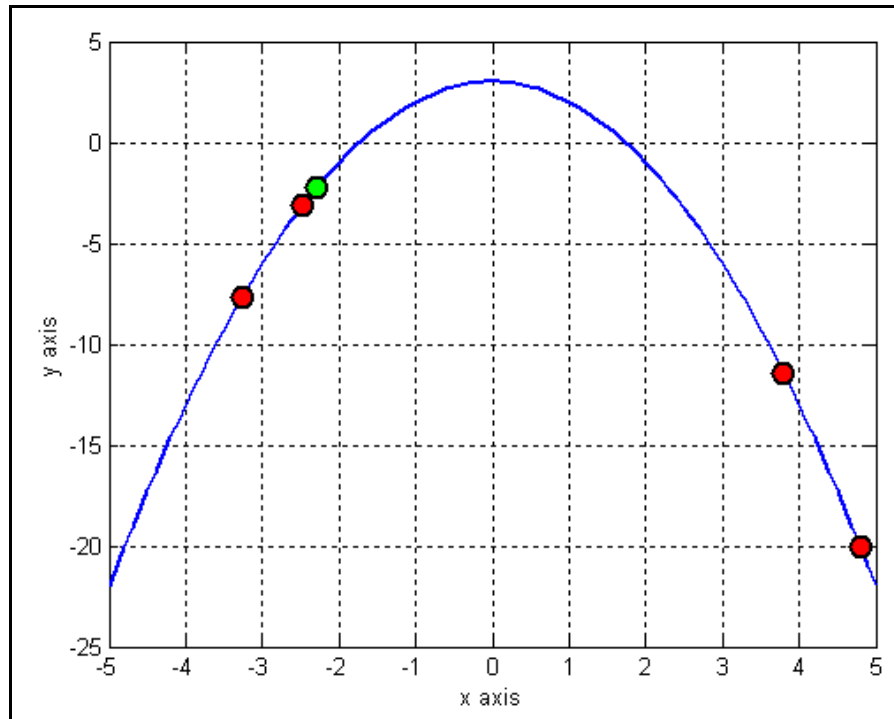


Figure 3.2 GA Solutions Plotted on Evaluation Curve

A termination condition statement follows the evaluation step. Here the GA determines whether to quit iterating or whether to continue on. Suppose that the GA continues since it is not satisfied with the current largest value for y .

In the selection process, one of the solution candidates for x is chosen to continue on. In this case it would be the solution that generated the green circle in Figure 3.2. This candidate is chosen to continue since its y value was the largest out of all the candidates.

Now the alteration/mutation takes place. The chosen candidate from the selection process is modified to generate five new candidates. This can be done by randomly generating 5 new values for x , where the randomly generated numbers vary by a magnitude of 1 with a mean equal to the chosen candidates x value.

These new candidates are then evaluated in (15) and the process returns to the condition statement. As the GA iterates through the loop structure, the Parent will have a tendency to

climb up the parabolic curve to the top where the solution resides. After many iterations, the Parent will tend to have a mean value of $x = 0$ and the new candidates will tend to be scattered between $x = -1$ and $x = 1$.

A complex GA will take much care in generating potential solution candidates during the alteration stage. If this is not done correctly, then the GA may not converge to the correct solution, or any valid solution at all for that matter. In the example presented above, a random perturbation of the current candidate is used to generate the new solutions.

Another common method of performing the alteration step is to use a crossover technique. The crossover is usually applied to pairs of Parents selected with a crossover probability. Since the example above only used one Parent, the crossover alteration was not performed. There are many types of crossover operators available in GA literature [35], and only few are outlined below. One-point crossover is the most basic operator, where a crossover point is selected at random so as to lie within the defining length of an individual, and to the right of this crossover point, portions of the two Parent individuals are swapped to create two new offspring Children. This method works well if the Parents are represented in a binary string as illustrated in the figure below.

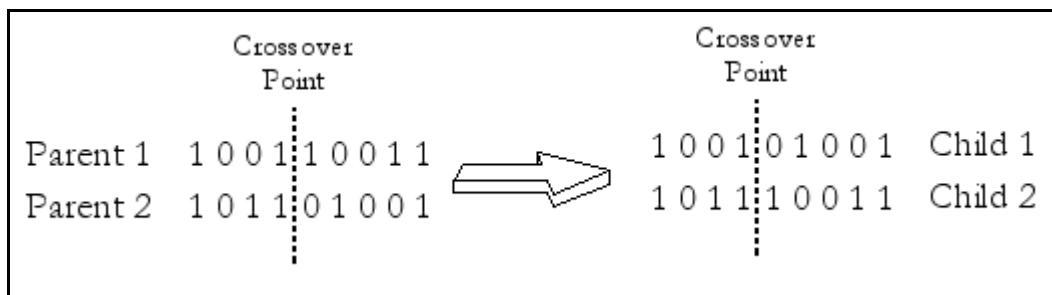


Figure 3.3 Crossover Operation

Two-point, and multi-point crossover [36] techniques are also common, and they only differ from the one-point crossover method by increasing the number of cross over points where the Parent data is swapped.

Arithmetical crossover [37] is used if the Parents are not represented as binary strings but rather as real-valued individuals. In this crossover operation, two individuals x_1 , and x_2 may produce two offspring Children, w_1 and w_2 by calculating a linear combination of their parents such as:

$$\begin{aligned} w_1 &= a \cdot x_1 + (1 - a) \cdot x_2 \\ w_2 &= (1 - a) \cdot x_1 + a \cdot x_2, \end{aligned} \tag{16}$$

where $a \in [0,1]$ as it always guarantees the correct bounds for w_1 and w_2 .

3.3 Using a GA to do Friction Modeling

The GA's optimization strategies can be taken advantage of to find the parameter values to different friction models. To do this, an evaluation criterion needs to be developed that will rate the Parent (t) at each generation t, to determine if it is a better or worse solution as compared to the previous solution, Parent (t-1).

3.3.1 Evaluation Criterion

Suppose a signal is sent to a motor, be it a voltage or a current, which causes the motor to turn. As the motor is turning, the angular position of the rotated shaft is collected through the use of an encoder mounted on the shaft of the motor. If the internal friction in the motor is high, then the input signal needed to move the motor will be much higher, as compared to the input signal sent to a motor that has low internal friction. Therefore, by monitoring the input signal and the output angular position, the friction in the motor can be characterized.

The hardware setup to do this is shown in Figure 3.4. The system has been connected in the standard closed loop position control configuration, seeing as the system in open loop is unstable. The input signal acts as the desired angular position that the shaft of the motor is commanded to reach. The output from the motor is the actual angular position that the shaft has rotated through. A position controller could be designed and placed in the feed-forward

path to improve the output response; however doing so would only hinder the friction model identification process since the friction characteristics would be masked inside the position controller. The reason for this is that, as more gain is added to the feed-forward path, the output from the motor becomes less sensitive to the input signal [38]. This is also the reason why unity feedback is used in the back loop. Larger feedback gains would also make the output from the system less sensitive to the input signals. Unity feedback was chosen as a compromise between no feedback and too much feedback.

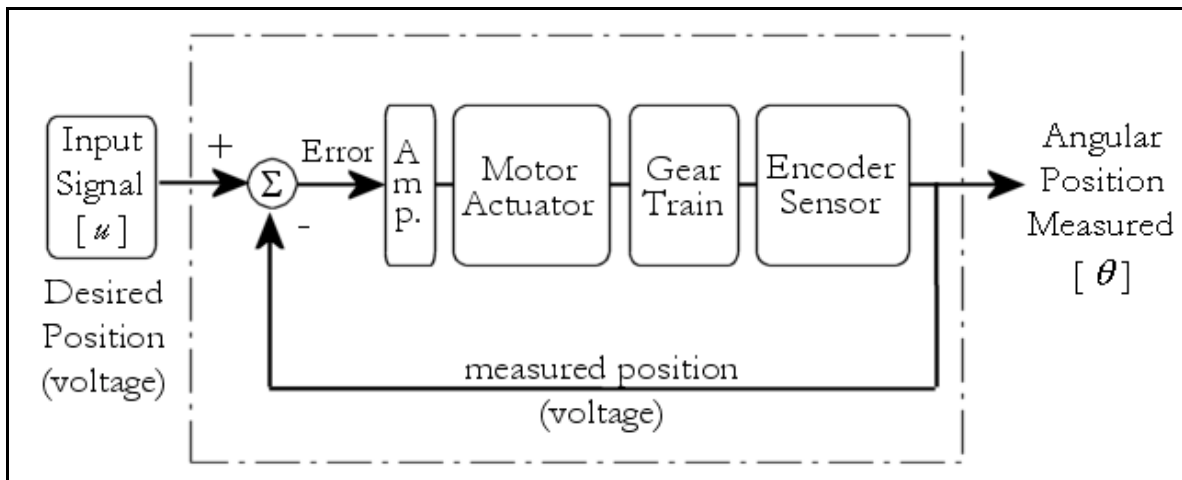


Figure 3.4 Real Data Collection Hardware Setup

After collecting the input and output data pair, the true angular position output needs to be compared with a simulated result to identify the parameters of a friction model. To collect the simulated data, the software setup shown in Figure 3.5 is constructed. The input signal used must be the same signal that was previously used for the true data collection. In simulation, a motor model and a friction model are needed before any data can be collected. The motor model should be relatively easy to acquire, since the control engineer should have a good idea of how the motor behaves. The friction model that is chosen can be any of the friction models that were shown in Chapter 2 or it can be just a mathematical function.

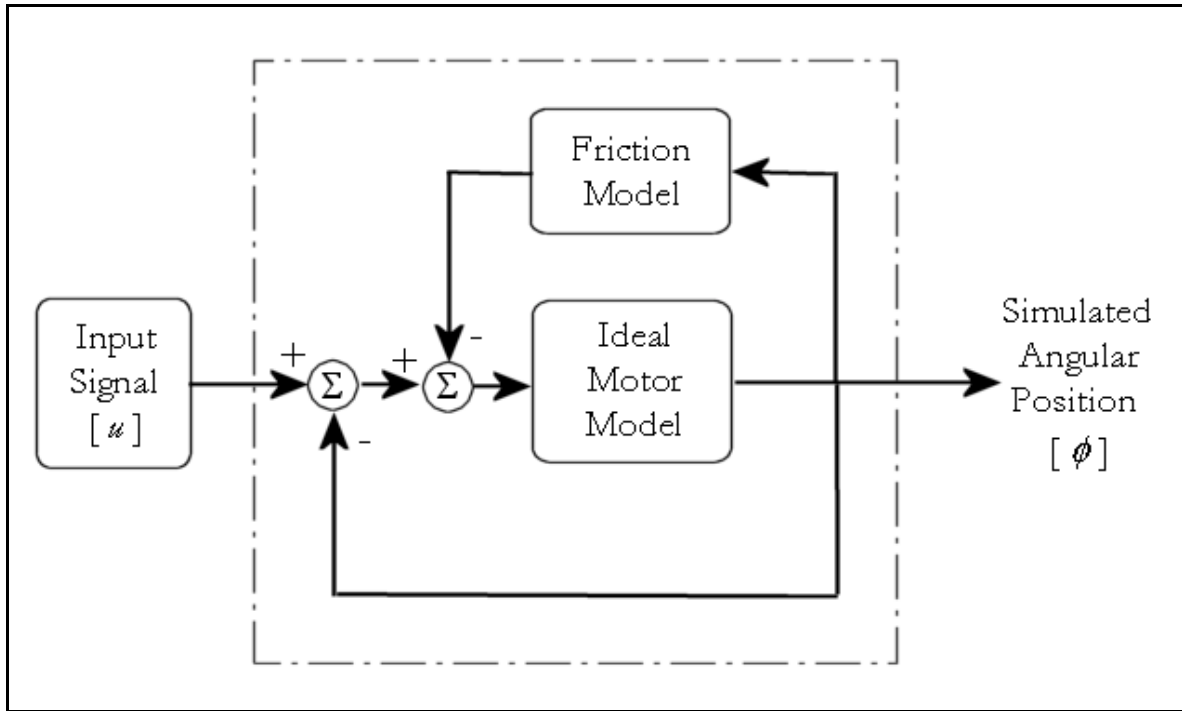


Figure 3.5 Simulation Data Collection Software Setup

The GA evaluation criterion is formulated using the diagram shown in Figure 3.6. The same input signal ($u[k]$) drives the real and simulated systems (the solid blocks shown in Figure 3.6 correspond to the dashed boxes illustrated in Figure 3.4 and Figure 3.5). The output from both the real system ($\theta[k]$) and simulated system ($\phi[k]$) is collected and analyzed to determine how well the friction model currently being used, fits the data. The analysis is done using the following equations.

$$Fit(P) = \sum_{k=1}^n (\theta[k] - \phi[k])^2 \quad (17)$$

$$Fit_{Best} = \min_P \{Fit(P)\}. \quad (18)$$

The GA's goal is to minimize the square of the difference between the real system output and the simulated system output over the whole data set n , by varying the friction model

parameters (P). For example, if the chosen friction model to be used was the Dupont model, then P would be the set containing the parameters $\{c_0, c_1, c_2, c_3, c_4\}$. The robustness of a GA allows one to modify the evaluation criterion to also include the motor model parameters inside the set P , if a clear motor model has not been defined. This way, the GA will attempt to find an optimal friction model *and* motor model that can characterize the overall system.

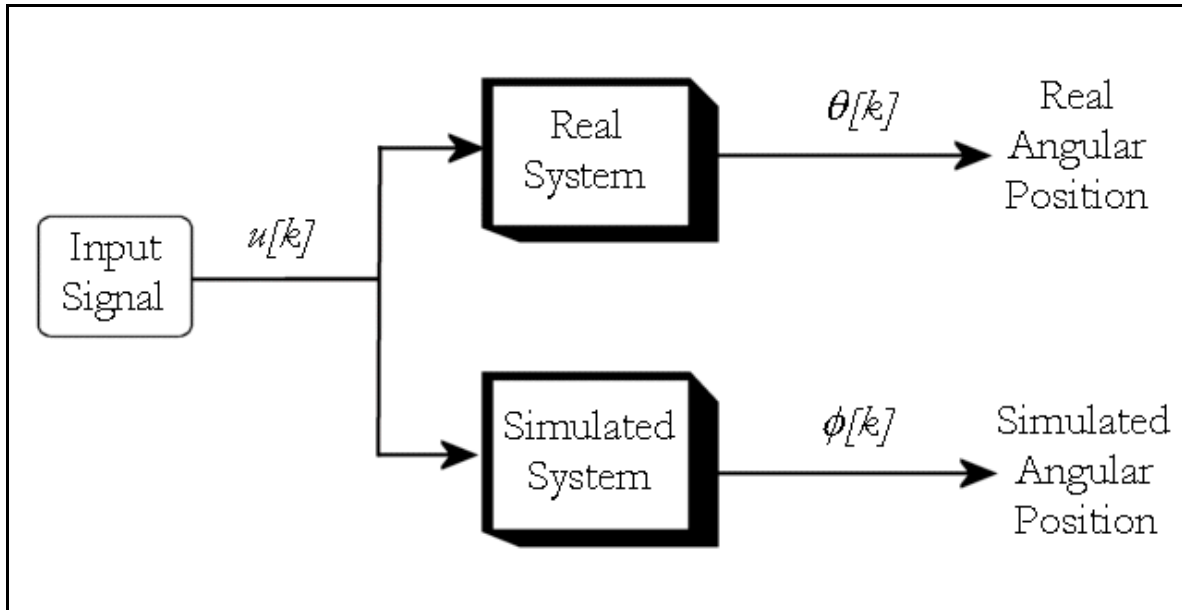


Figure 3.6 Evaluation Criterion Setup

3.4 Summary

This chapter discussed a method that could be used to identify friction model parameters with the use of a genetic algorithm, and background information is presented on the structure and optimization capabilities of a genetic algorithm. The next chapter dives into the specific workings of the designed Genetic Algorithm that is used to perform the friction model parameter identification.

Chapter 4

Genetic Algorithm Details

The general structure of a GA was described in the previous chapter. This chapter discusses the details of the inner workings of the GA that has been developed to do friction modeling for the purpose of friction compensation. A GA was chosen to be used since formulating the friction modeling problem is relatively straight forward, as will be shown in Section 4.1.5, and the optimization benefits of a GA are ideal for finding the parameter values in the non-linear friction models presented in Chapter 2.

4.1 Sequence of GA Operations

There are six steps that are followed when creating a friction model with the GA. These steps are outlined below:

1. Collect real input & output data pair from the motor
2. Select a motor model structure
3. Select a friction model structure
4. Setting other GA parameters
5. Run the GA
6. Analyze the results and return to step 2 if necessary

4.1.1 Collecting Real Input & Output Data Pair

The first step, collecting experimental data, is very important. The data that is collected determines which regime the final friction compensated system will work well in. If the motor is excited at a high frequency during data collection, then the friction compensated system should work well under the same conditions. However, if the friction compensated system is operated at a low frequency, then the friction compensator may not work as well.

There is an upper bound to the maximum frequency at which a motor can operate at, and if the motor is excited with a frequency which is too high then it will cease to respond. The motor could even become permanently damaged.

The amplitude of the input signal also greatly affects the quality of the output that will be collected since friction is nonlinear. The output depends on both the frequency and the amplitude of the input signal. In particular, with a motor which contains a high degree of internal friction, the amplitude of the input signal will need to be large to initiate motion. Small amplitude signals will not create any motion; therefore this data would not be very useful when used in the GA.

A good input signal to use is one which causes the motor to move through its regular operating range as defined by its application. An example of an input signal that can do this is a decreasing amplitude chirp signal. This signal is comprised of two parts to account for both frequency and amplitude effects. The first part is a regular chirp signal which starts at a low frequency (0.05 Hz) and slowly increases in frequency to 0.4 Hz over 100 seconds. The second part is a ramp signal which begins at an initial value of 1, and decreases slowly down to zero with a slope equal to -0.01. These two signals are multiplied together to give the result shown in Figure 4.1.

The initial frequency of the chirp signal should be low enough so that the motor has enough time to react before the input signal changes sign. The amplitude of the input also needs to be large enough to initiate motion. Under position control, it is recommended that the amplitude of the input causes the motor to turn at least 180 degrees.

The rate of increase in the frequency and the decreasing rate of the amplitude of the input signal should result in the motor ceasing to move near the end of the desired data set. The termination of motion should be the result of the input signal being too low in amplitude rather than too high in frequency. This will ensure that the motor will not sustain any damage during data collection.

An input signal which has a high frequency, large amplitude start and a low frequency, small amplitude finish, would not be very useful seeing as the motor would not move very. The high frequency, large amplitude signal, would not give the motor enough time to react before the input signal changes direction. The low frequency, small amplitude signal would not have enough energy to drive the motor to move due to static friction. It is therefore better to sweep the frequency from low to high as the amplitude of the input is reduced.

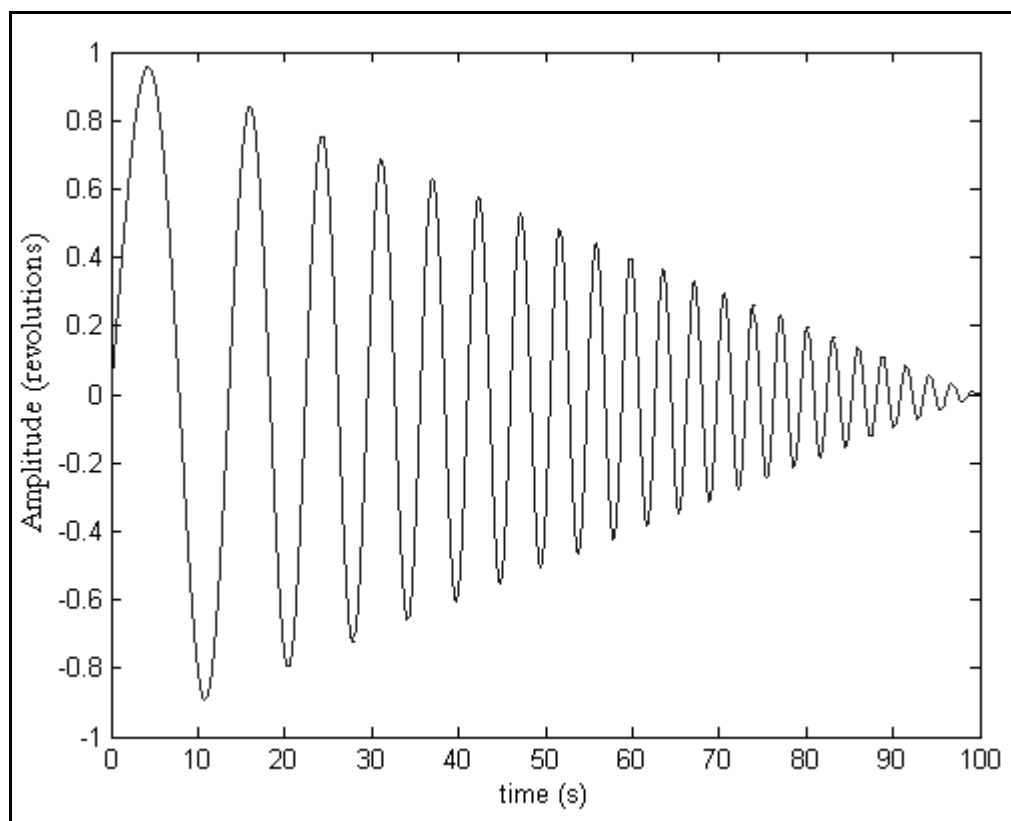


Figure 4.1 Decreasing Amplitude Chirp Signal

4.1.2 Motor Model Structure

Step 2 states that a motor model structure has to be selected next. In the absence of friction, a simple linear motor can be modeled as,

$$\frac{\theta(s)}{u(s)} = \frac{K_m}{J \cdot s^2 + B \cdot s}. \quad (19)$$

Here J represents the motor moment of inertia, B represents the viscous damping constant and K_m represents the torque constant of the motor. $\theta(s)$ and $u(s)$ are the Laplace domain equivalent of the angular rotation of the motor shaft and the input to the system, respectively. If the motor contains gears then the gear ratio can be absorbed into the motor model parameters.

By dividing both numerator and denominator by K_m , the model can be simplified to the following equivalent,

$$\frac{1}{J_m s^2 + B_m \cdot s}. \quad (20)$$

There are now only two parameters that are needed to identify this motor model completely, where three parameters were required in (19). This simplification is done to increase the speed of execution of the GA.

The GA is not restricted to only using (20) as the motor model; however, this equation is convenient to use since it is linear and designing a controller for a linear system is easy to do.

4.1.3 Friction Model Structures

The GA has been pre-programmed to contain five different friction models, which can be used to model the friction in a real system. Table 4.1 summarizes the friction models found in Chapter 2. All the models shown in this table have been pre-programmed into the GA except

the LuGre model. The difficulty with using the LuGre model is that it contains a differential equation of the variable z . This variable represents an immeasurable quantity (elastic deformation of asperities in contacting surfaces), therefore making it very difficult for the GA to converge to a solution for the parameter values. Tests were performed by collecting simulated data for a motor with friction. Using this collected data, the GA was run to see if it could converge to the solution of the friction model which was used during the simulation. Only the LuGre model could not converge to the correct solution; therefore, it is recommended to only use the GA on friction models which are expressed by non-differential equations.

During each run of the GA, only one friction model may be selected to be used at a time. Section 4.1.6 describes how to analyze the results of the GA to determine which friction model is the best solution.

Table 4.1 Summary of Friction Models

	Pre-Sliding	Stick-Slip	Sliding	Stiction	Coulomb	Viscous	Varying Break-away Force
Exponential		√	√	√	√		
Tustin			√	√	√		
Non-Linear				√	√	√	
Dupont			√		√	√	
7-Parameter	√	√	√	√	√	√	√
LuGre	√	√	√*	√*	√*	√*	√
* This characteristic depends on the parameterization of the function $g(v)$							

The five selected friction models to be used in the GA are listed below with their accompanying equations. Some of the models have been modified slightly as compared to

their representations in Chapter 2, to make them easier to implement in a control strategy and to make them characterize as many friction regimes as possible.

4.1.3.1 Exponential Friction Model

The model shown in (6) attempts to model the Stribeck effect. To simplify the model for use in the GA, the dependence of the friction model on acceleration and deceleration of the moving bodies is eliminated by removing one of the equations from (6). Removing one of these equations has a negative effect on the friction model since the model loses its capability to model stick-slip. However, with only one equation, this model is now much easier to implement into a control strategy. To complete this model and allow it to model viscous friction, a viscous component (σ) is added. The resulting friction model is,

$$F_{Exponential}(v) = \left(F_{k\min} + (F_{ST} - F_{k\min}) \cdot e^{-(\gamma|v|)^\delta} + \sigma \cdot |v| \right) \cdot \text{sgn}(v). \quad (21)$$

$F(v)$ is the friction force; $F_{k\min}$, F_{ST} , γ , δ and σ are positive constant values that parameterize the model, and v is the relative velocity between the moving surfaces.

The resulting model now has the capabilities to model the characteristics shown in Table 4.2.

Table 4.2 Exponential Friction Modeling Capabilities

	Pre-Sliding	Stick-Slip	Sliding	Stiction	Coulomb	Viscous	Varying Break-away Force
Exponential			√	√	√	√	

4.1.3.2 Tustin Friction Model

The model shown in (7) was also developed to only model the Stribeck effect. It was found by Armstrong through experiments that this model could be further generalized to fit different kinds of experimental data by adding an exponent (x) to one of the terms [10,21]. Doing so enables this friction model to characterize sliding. Adding a viscous component (σ) to model viscous friction also helps to complete the model to be used in the GA. The final equation for the Tustin model is,

$$F_{Tustin}(v) = \left(F_{f0} - F_{fc} \cdot \left[1 - e^{-\left(\frac{|v|}{V_c}\right)^x} \right] + \sigma \cdot |v| \right) \cdot \text{sgn}(v). \quad (22)$$

$F(v)$ is the friction force; F_{f0} , F_{fc} , V_c , x and σ are positive constant values that parameterize the model, and v is the relative velocity between the moving surfaces.

The resulting model now has the capabilities to model the characteristics shown in Table 4.3.

Table 4.3 Tustin Friction Modeling Capabilities

	Pre-Sliding	Stick-Slip	Sliding	Stiction	Coulomb	Viscous	Varying Break-away Force
Tustin			√	√	√	√	

4.1.3.3 Non-Linear Friction Model

The model shown in (8) is complete in the sense that it models all the friction regimes that are of interest. Therefore, no modifications are made to it. The model is shown again below for completeness;

$$F_{Non-Linear}(v) = \left(\alpha_0 + \alpha_1 \cdot e^{-\beta_1 \cdot |v|} + \alpha_2 \cdot \left(1 - e^{-\beta_2 \cdot |v|} \right) \right) \cdot \text{sgn}(v). \quad (23)$$

$F(v)$ is the friction force; α_0 , α_1 , α_2 , β_1 , and β_2 are positive constant values that parameterize the model, and v is the relative velocity between the moving surfaces.

This model has the capabilities to model the characteristics shown in Table 4.4.

Table 4.4 Non-Linear Friction Modeling Capabilities

	Pre-Sliding	Stick-Slip	Sliding	Stiction	Coulomb	Viscous	Varying Break-away Force
Non-Linear				√	√	√	

4.1.3.4 Dupont Friction Model

Similarly the model shown in (9) is also complete in the sense that it models all the friction regimes that are of interest. No modifications have been made to it either. The model is presented below for completeness;

$$F_{Dupont}(v) = \left(c_0 + c_1 \cdot |v| + c_2 \cdot e^{-\left(\frac{|v|}{c_3} \right)^{c_4}} \right) \cdot \text{sgn}(v). \quad (24)$$

$F(v)$ is the friction force; c_0 , c_1 , c_2 , c_3 , and c_4 are positive constant values that parameterize the model, and v is the relative velocity between the moving surfaces.

This model has the capabilities to model the characteristics shown in Table 4.5.

Table 4.5 Dupont Friction Modeling Capabilities

	Pre-Sliding	Stick-Slip	Sliding	Stiction	Coulomb	Viscous	Varying Break-away Force
Dupont			√		√	√	

4.1.3.5 Seven-Parameter Friction Model

The last model that is available for selection in the GA comes from (11), (12) and (13). Since, during pre-sliding motion, the system only moves on a microscopic scale, (11) can therefore be ignored. This leaves the following equations to define this friction model;

$$F_{7\text{parameter}}(v) = F_{co} + F_{vs} \cdot |v| + F_{SF}(\gamma, t_2) \cdot \frac{1}{1 + \left(\frac{v \cdot (t - \tau_L)}{v_s} \right)^2}$$

where

$$F_{SF}(\gamma, t_2) = F_{s,a} + (F_{s,\infty} - F_{s,a}) \cdot \frac{t_2}{t_2 + \gamma} \quad (25)$$

$F(v)$ is the friction force; F_c , F_v , τ_L , v_s , γ , and $F_{s,\infty}$ are positive constant values that parameterize the model. $F_s(\gamma, t_2)$ is the magnitude of the Stribeck friction constant, $F_{s,a}$ is the magnitude of the Stribeck friction constant at the end of the previous sliding period, t_2 is the dwell time and v is the relative velocity between the moving surfaces.

The resulting model now has the capabilities to model the characteristics shown in Table 4.6.

Table 4.6 Seven-Parameter Friction Modeling Capabilities

	Pre-Sliding	Stick-Slip	Sliding	Stiction	Coulomb	Viscous	Varying Break-away Force
7-Parameter		√	√	√	√	√	√

4.1.4 Setting other GA Parameters

The GA is set up to run with an initial population size of one or greater. Each individual in this population is called a Parent. A Parent represents one solution set for the friction model and motor model parameters.

With each progressing generation, each one of the Parents will generate a new set of solutions to be evaluated. These new solutions are called the Children. Once all of the Children have been evaluated, if any one of the Children contains a solution which is better than their Parent solution, then that Child will replace their Parent for the next generation.

The method which is used to generate new Children depends on a variable g which represents the number of generations that the Parent has existed for. The way in which g works is described in 4.1.5. The value of g was chosen by trial and error to be equal to four for all the work done in this thesis.

The number of Parents and Children to use in the GA needs to be specified before the GA is started. These numbers determine how efficient the GA will be in searching the entire solution space for an optimal solution. Each Parent searches for a solution on its own. Therefore, the more Parents performing searches, the higher the probability of finding a global optimal solution rather than finding just a local solution.

A large number of Children increases each of the Parent's search capabilities. Each Child is spawned from a Parent, and if a Parent solution set resides close to the optimal solution,

having a large number of Children will reduce the number of generations required to converge to the optimal solution. The downfall of having a large number of Parents and/or Children is that more computation time is required for each generation to be processed.

Besides specifying how many Parents to start the GA with, each Parent solution set needs to be initialized to some value. Each of the Parent solution sets, P , consists of the following parameters. Here, n represents the number of different parameters needed to fully characterize the friction model of interest.

$$P = \{p_1 \dots p_n, J_m, B_m\}. \quad (26)$$

The friction model parameter values are specified by p_1 through to p_n , and the motor model parameter values are specified by J_m and B_m .

Initializing each of the values in the set P can be done one of two ways. The first way is to specify manually each of the values for all of the Parents. This method would be preferred if the user would like to have total control of where the Parents start in the solution space. The second way to initialize P is to specify a range for each of the parameters within P , and have a computer randomly generate each of the values. This second method is preferred over the first since it will generate a random sampling over the solution space to initialize the GA. There won't be any bias to one location in the solution space.

Another GA parameter that needs to be specified is the termination condition value. This value notifies the GA to stop iterating once a solution has reached sufficiently close to the desired answer. The desired solution is one which models the experimental output behavior of the motor perfectly, through simulation. The model's *fit* value is calculated based on (17). The square of the difference between the experimental data and the simulated data over the whole data set, gives a measure of how well the Parent parameters model the friction in the system under test. Smaller *fit* values correlate to better models of the experimental system. A Parent which models the system perfectly would have a *fit* value equal to zero, since the simulated and experimental data would be equal.

The termination condition value is determined by a trial and error process. Initially the value is set to zero, since the ideal solution is what is desired. The GA is left to run for a long time and the rate of change, ϵ , of the *fit* value is analyzed. If the ϵ is equal to zero for more than a few hundred iteration then the GA is said to have converged. The termination condition can be set for subsequent runs equal to the *fit* value of the converged solution.

The last GA parameter that needs to be set specifies which models the GA is asked to identify. Since P incorporates both the friction model and the motor model parameters, there may be times when only the friction model is desired as opposed to the motor model or visa-versa. Other times a friction model and motor model may be required. Therefore, this last GA parameter determines which parameter values of P to alter during each generation when creating new Children. When the GA is run for the first time on a system, it is recommended to allow the GA full flexibility in choosing both the motor model and friction model parameters. This freedom will result in the GA converging to a solution in the least amount of time.

4.1.5 Running the GA

Once the GA parameters have been specified, the first generation can begin. A flow chart of the GA's internal operations is shown in Figure 4.2.

The first thing that the GA does is it initializes all the Parents by generating a set of specific values for each solution set, P . This initialization is done according to the description in section 4.1.4. The values within P represent the friction model and motor model parameter values.

The next step in the GA is to evaluate each of the Parents. The evaluation is done by taking the collected experimental data and comparing it with a simulated result that is generated based on each of the Parents solution set P . Figure 4.3 shows a block diagram of the simulation environment that is used to generate the simulation results.

Each Parent's solution set P is applied to the simulation environment, and the output (ϕ), is generated based on the same input signal that was used when the experimental data was collected. The simulated output data is compared to the experimental output data (θ) and a *fit* value is assigned to each Parent in accordance to (17).

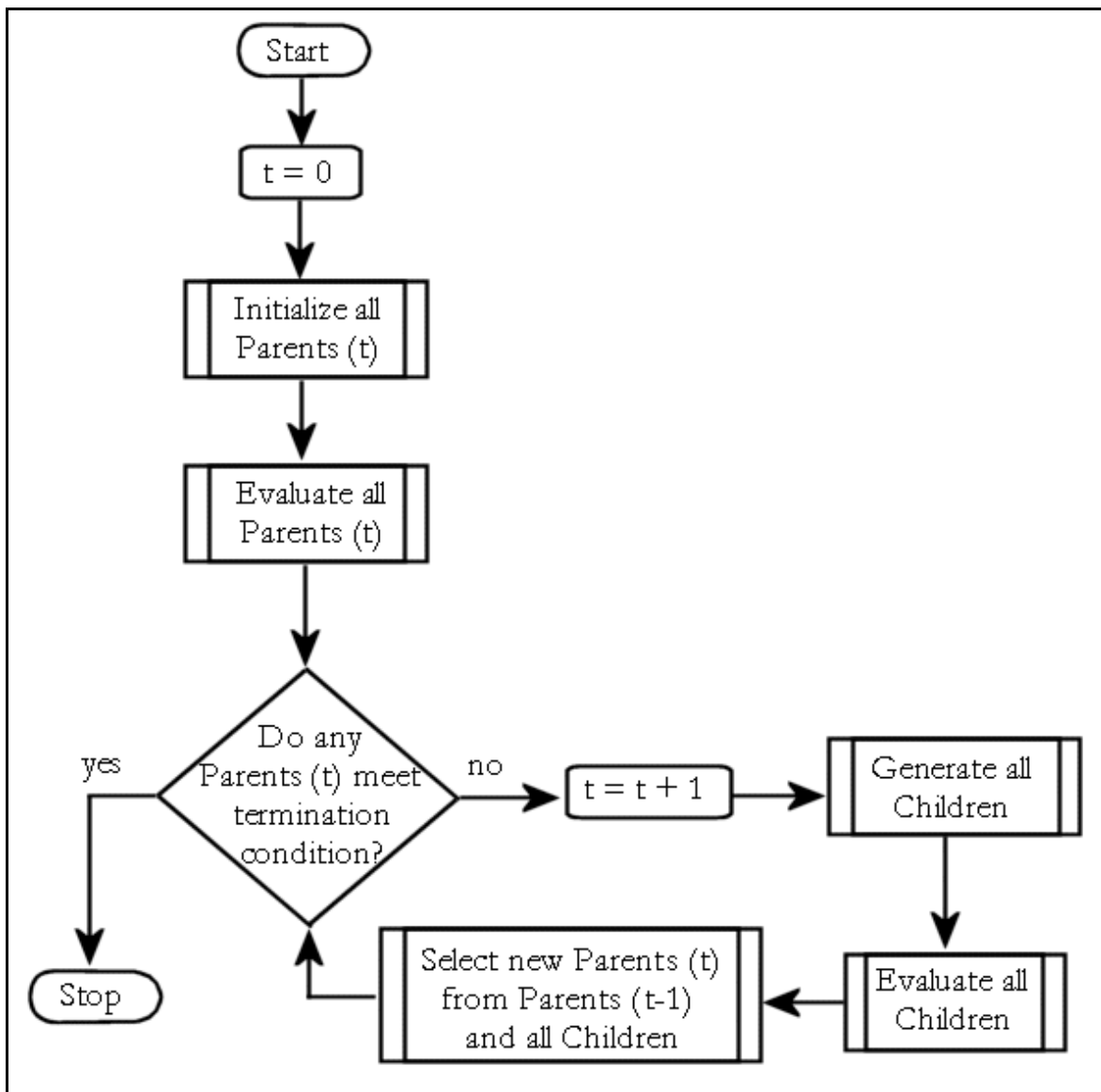


Figure 4.2 Flow Chart of GA

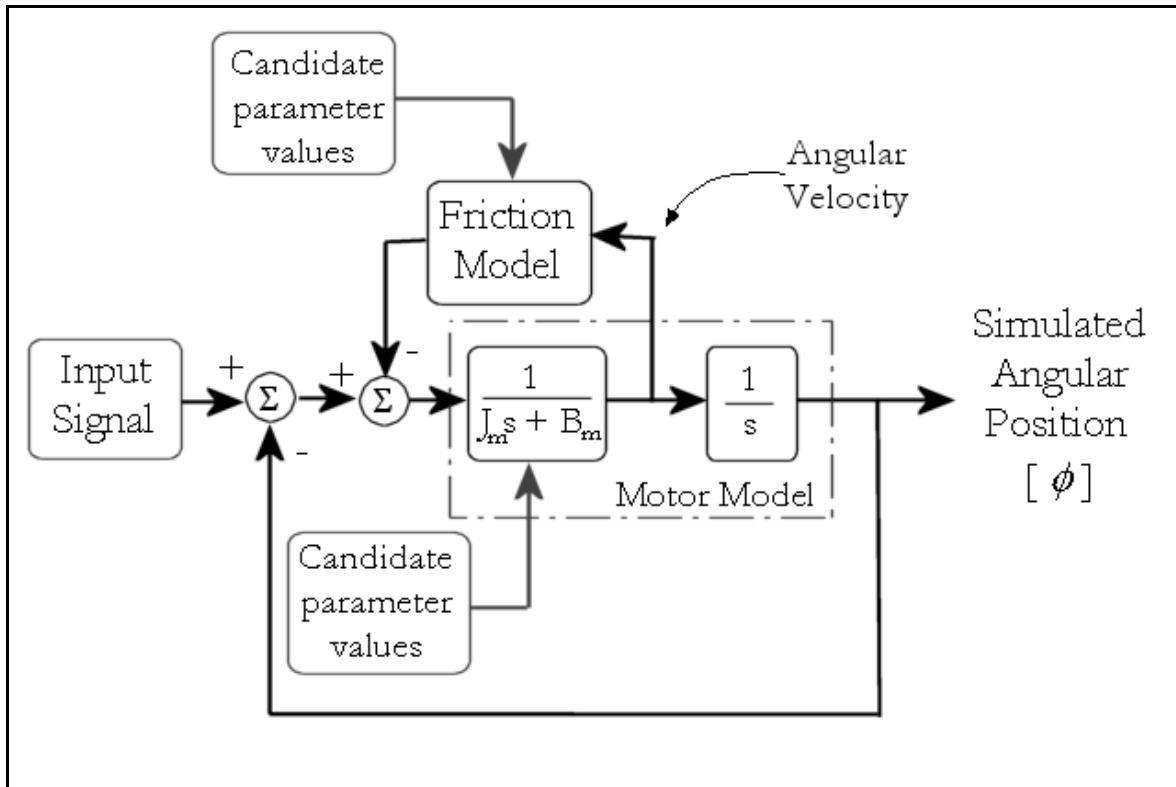


Figure 4.3 Simulation Environment

After the evaluation stage, the GA flow progresses to the termination condition statement. Here, all the Parent *fit* values are compared to the termination condition value which was specified during the GA setup. If any of the Parent *fit* values are less than or equal to the termination condition value, then the GA will terminate its execution. If this condition is not met, then the GA will proceed through to the next iteration loop and generate another set of solutions.

Each iteration begins with the creation of new Children based on the current Parents. The Child creation process has been designed to allow the GA to search the entire solution space for the most optimal answer. The method used to create the new Children is dependent on how many generations the Parent has survived through. If the Parent is relatively young, meaning that it has only progressed through less than g generations, then the method which is used to create the new Children is the one to be described in 4.1.5.1. If the parent has existed

for greater, or equal to g generation, then the Child creation process which is used is the one to be described in 4.1.5.2. This value results in the GA converging in a relatively short period of time, during tests.

Two different methods are used to generate new Children because as the solution set P , converges to the ideal solution, fewer parameters need to be adjusted to continue converging. This was discovered through simulation tests that were run while validating that the GA has the capability to converge to the correct solution. Without the second method to generate new Children, the GA would still converge, however it would require many more generations to obtain the same results.

4.1.5.1 Child Generation Using Young Parents

All the parameters in the Parent's solution set P , are taken and perturbed slightly. These new parameter values form the solution set C which belong to the Child. The perturbation which is performed on each parameter is done according to a normally distributed random number with a mean μ , and a standard deviation σ . A normally distributed random number is used because a perturbation generated this way ensures that the Child will still be closely related to the Parent. However, it will contain a unique solution. Refer to Appendix A for calculations of μ and σ for a uniform random variable.

Using the results from (29) and (33) in Appendix A, μ and σ can now be defined for the normally distributed random number which is generated for each of the parameters in the set C . Since μ represents the midpoint of the interval for a uniform random variable, the parameter value from the set P is chosen to be equal to μ for each of the newly created normally distributed random numbers. This ensures that the Child parameter values being created are close to the original Parent parameter values.

The value for σ is calculated based on the following equation,

$$\sigma = \left(\frac{(Param_{max} - Param_{min})}{\sqrt{12}} \right) \cdot Random(0..1). \quad (27)$$

$Param_{max}$ and $Param_{min}$ represent the current parameter's maximum and minimum value range. These values were specified during the setup stage of the GA. If the parameter was fixed to one value during initialization, then the quantity $(Param_{max} - Param_{min})$ in (27), is set equal to 1. The random number generated between 0 and 1 ensures that the normally distributed random numbers generated for the Children are as diverse as possible, but yet correlated to the Parent values. If any of the new parameter values which are generated for the set C are negative, then they are converted to be positive by changing their sign. This is done to guarantee that only feasible solution will exist in the set C . It is also possible that a new parameter value may be set to zero, thereby resulting in a divide by zero error in some of the friction models. These occurrences should be handled appropriately to avoid numerical problems, for example, discarding solution sets which would cause divide by zero errors.

In addition to this mutation in parameters, a crossover operation is performed at random intervals. During a crossover operation, two random parents are selected and their parameter values are crossed over in accordance to the arithmetic crossover operation described by (16).

4.1.5.2 Child Generation using Older Parents

Instead of generating new parameter values for *all* of the parameters within the set C , only one randomly selected parameter is perturbed. All of the other values within the set C are inherited from the Parent set P . The method used to generate the new value for the one parameter that is selected to be changed, is the same as described in Section 4.1.5.1.

After the Children have been generated, then they are run in the simulation environment to find their individual *fit* values according to (17). The Children who have *fit* values which are smaller than their Parents *fit* value, replace their Parents for the next generation loop. All the new Parents are tested against the termination condition value and the process loops again.

4.1.6 Analyzing results from the GA

There may be times when the GA is run, but a solution is not achieved because the GA does not converge. If this occurs, it is recommended to abort the GA and start a new run using a different friction model. Restarting the GA with the same friction model may sometimes also help, if a new range is specified for each of the model parameters. This can help because the GA will initialize the Parents to a different location in the solution space as compared to the first run.

Tightening the range over which the model parameters can initialize to, will also help in converging to a solution. However, if there is no prior knowledge about what values the parameters could be, then tightening the range will not be useful.

When starting to work on a system that is previously unidentified, it is strongly recommended to allow the GA to have full flexibility in choosing the friction model and motor model parameters in each generation. Restricting the GA to only look for a motor model or just a friction model should be left to the end when fine-tuning of the models is desired.

Once the GA converges to a solution with one friction model, that model's shape can be used to help other friction models converge faster. The converged friction model's frictional force versus velocity characteristic can be plotted and used to determine how to initialize the GA to find solutions for the other friction models. Through trial and error, a range of values can be identified for use with the other friction models so that a similarly shaped friction characteristic will be created. These ranges of values can be used to initialize the GA to find different solutions for the other friction models.

Achieving a good friction model to use in a control strategy requires an iterative approach to the problem. First, one friction model needs to be found. Once one model is attained, then its shape characteristics can be used to find other friction models as described above. After a collection of different converged friction models have been obtained, the model with the smallest *fit* value represents the *best* friction model that matches the collected data. Further convergence may be obtainable by using the shape characteristics of the *best* model to re-

initialize the other, already converged, friction models. Assuming that the *best* model is not the same friction model as the first one to be found, the re-initialization could result in finding better parameterizations for the other friction models.

After finding the best friction model according to its *fit* value, the friction model still needs to be tested. Testing the model involves setting up a closed loop system, to be described in Chapter 5. An input signal is applied to the closed loop system, and the input and output to the motor with friction is observed. The input signal should differ from the original input signal used in collecting the input and output data for the GA.

If the output does not show signs of improved performance with the friction compensator in place, then a different friction model should be used. It may be necessary to collect an entirely new set of input and output data to achieve a better friction model. Chapter 5 discusses in more detail how to use an identified friction model for purposes of friction compensation.

4.2 Genetic Algorithm Summary

This chapter discussed the internal workings of the designed GA. A description of the motor model and friction models that are used in the GA were presented and an overview of the simulation environment was outlined. Finally the GA flow structure was analyzed and a description was given for each of the major sections within; initialization, evaluation, termination condition, and Child generation. Lastly, pointers on how to make the GA converge to a good solution were given.

The next chapter discusses how to use the results from a successful run of the GA to perform friction compensation on the identified system.

Chapter 5

How To Use The GA Results

This chapter outlines the procedure to follow to successfully implement a friction compensation technique using the results gathered from the GA. This friction compensation technique is then used on a harmonic drive to demonstrate that the motor gains improved performance.

5.1 Friction Compensation Methodology

The GA that has been developed models the motor and friction as two distinct blocks. One block represents the motor model and the other block represents the friction model. These two blocks interact with one another as shown in Figure 5.1. The dashed box shown in Figure 5.1 represents the real motor under test.

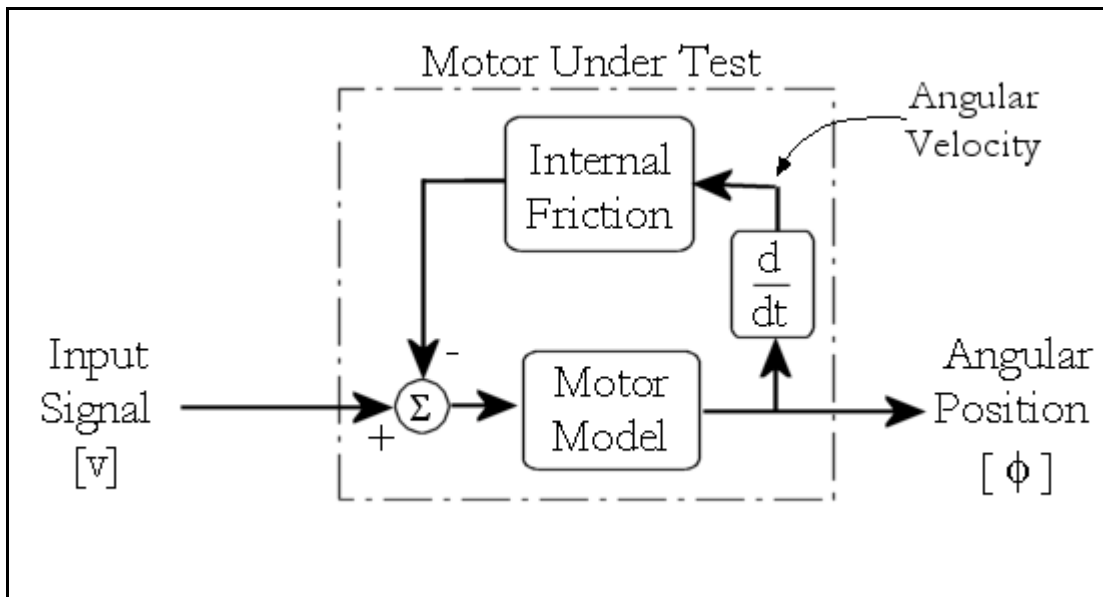


Figure 5.1 Model of the Motor Under Test

The structure illustrated above shows that an input signal v is reduced by the friction before it is used to drive the motor model. This reduction of the input signal is what causes the motor to behave as if it is under the influence of friction.

To compensate for the frictional effects, the structure shown in Figure 5.2 is used. The GA identified model used to characterize the internal friction in the motor is used in a feedback loop to *add* to the input signal. This extra addition to the input signal is used to counteract the internal friction within the motor. If the friction model matches closely the true internal friction of the motor, then the overall effect of the system will be approximately linear and equivalent to the motor model without any friction.

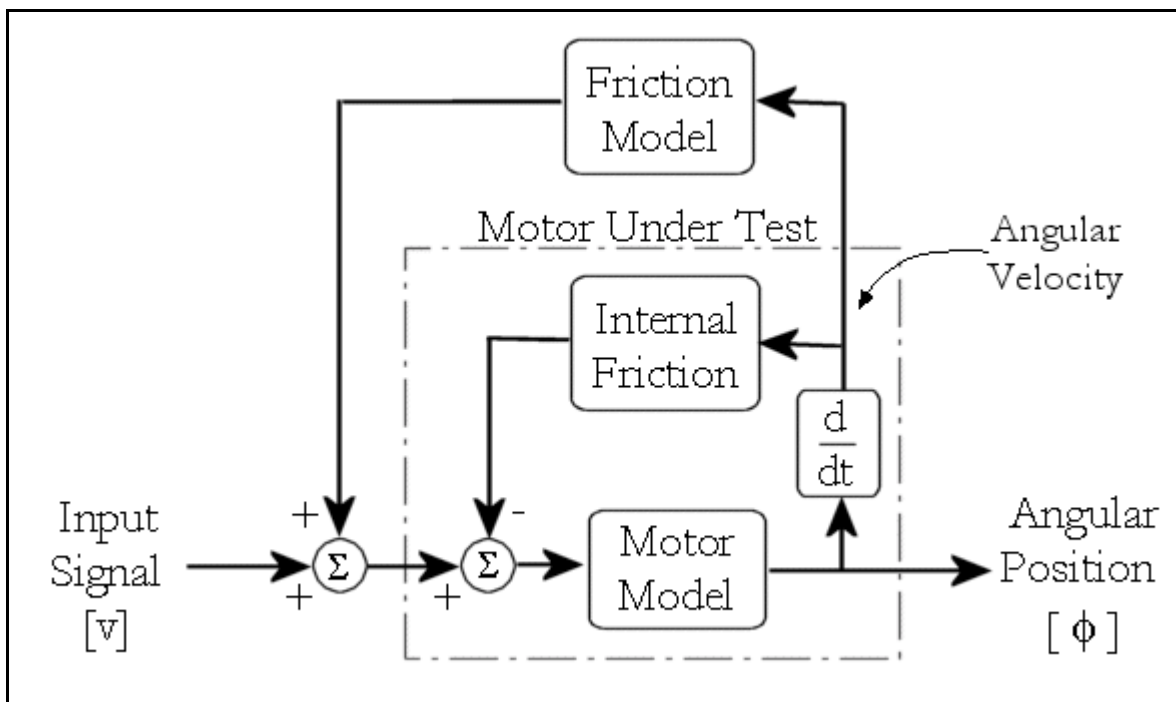


Figure 5.2 Friction Compensation Setup

5.2 Limitation of the Friction Compensator

Even though the GA may be able to model the motor under test very closely, most likely the resulting model will not match exactly to the real system dynamics. This can pose problems when performing friction compensation since the internal friction inside the dashed box and the friction model outside the dashed box will be different. It is therefore possible for the feedback friction compensator to destabilize the overall system. If the friction model overestimates the true internal friction, then the friction model could cause the motor to move even if the input signal is zero, for example, the friction compensator may act as a negative friction, effectively pushing the system. To prevent this from happening, it is advisable to scale down this feedback signal by 90%-95% of the entire value in the feedback loop. The exact percentage should be determined through experimental analysis.

Since all the friction models that are used by the GA depend on velocity, it is very important to calculate the angular velocity of the motor carefully. Lost data bits from an encoder will create problems when the position signal is differentiated to get the velocity. Each lost piece of data in the position signal will show up as a large spike in the velocity signal. This is a problem because large velocity spikes will correlate to large frictional forces being fed back. These large feedback signals from the friction model will increase the input signal up towards saturation.

Noise in the position data can also make it difficult to calculate the velocity. A filter should be used on the position data to smooth it out if it is noisy, so that the velocity signal does not contain any erratic behavior. A filter may introduce lag on the feedback compensation signal, thus degrading the performance of the friction compensator. It is therefore important to maintain synchronization of the input signal with the feedback signals for the friction compensator to work in real-time.

5.3 Experimental Results

To demonstrate that the GA can be used to develop a friction compensator, a simple experiment was employed. A large harmonic drive actuator was used as the motor under test as illustrated in Figure 5.3. Details on the internal workings of a harmonic drive are given in Appendix B. A block diagram of the experimental setup is shown in Figure 5.4 and the equipment used is summarized in Table 5.1.

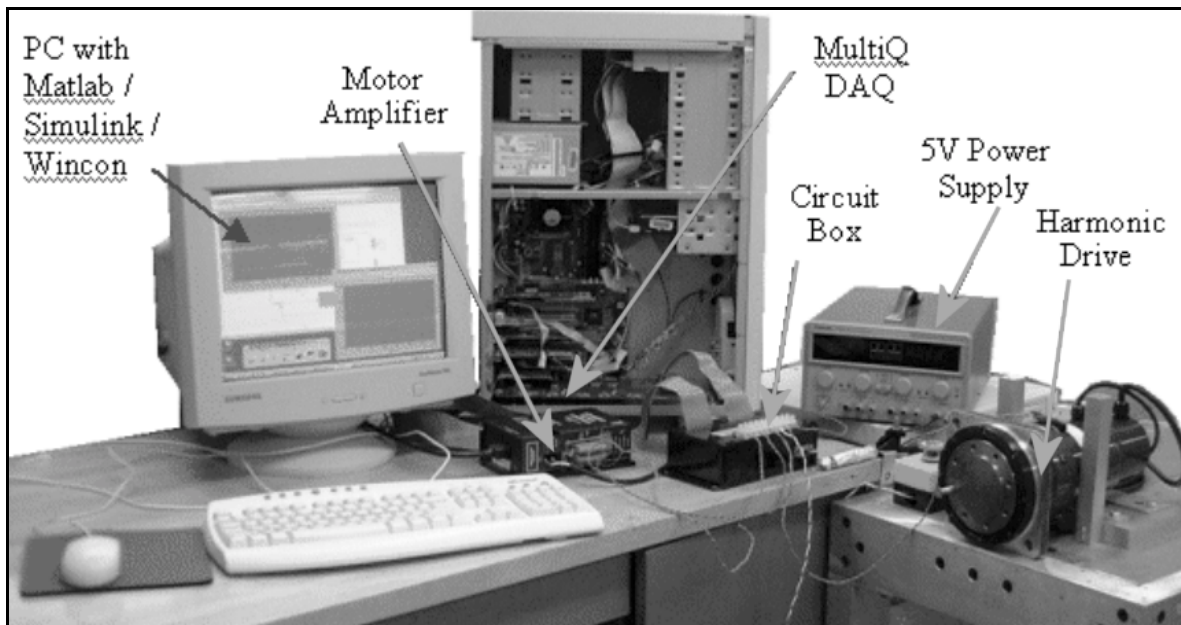


Figure 5.3 Experimental Setup

Everything inside the dashed box in Figure 5.4, was realized in hardware, and everything outside the dashed box was created in software in the Simulink environment in Matlab. The amplifier located between the DAC and the motor acts as a straight gain, thus its effect on the overall system is modeled together with the motor model. A saturation block is placed before the DAC to avoid any damage to the DAC hardware, and the filter located in the feedback loop with the friction model, replaces any lost encoder bits with the data from the previous collected sample. The encoder data from the motor did not contain very much noise therefore; no additional filtering needed to be performed. Additional lag was not introduced into the feedback signal through the use of the filter.

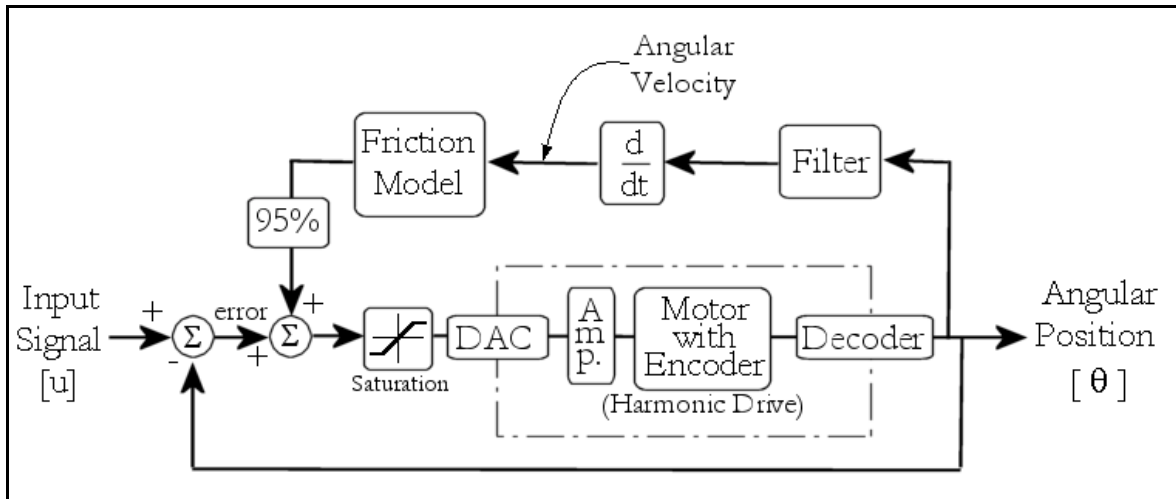


Figure 5.4 Experimental System Block Diagram

Table 5.1 Equipment

Equipment	Description	Function
Amplifier	Advanced Motion Controls 30A20AC	Amplify control signal to be used by Harmonic Drive
Circuit Box	Misc. Hardware	Used to interface DAC to hardware, and decoder to software
Computer	Pentium 3, 800 Mhz	Location where all software resides
DAQ	Mult-Q 2	DAQ Hardware
Harmonic Drive	HD Systems RFS-32-6030	Motor Actuator with high internal friction and encoder
Power Supply	5 Volt Supply	Used to power Circuit Box and encoder
Software	Matlab v6.0 Simulink v4 WinCon v2	Software for control & simulation environment, and DAQ software

The 95% scaling factor located on the output of the friction model was determined by experimentation. 95% was decided upon because this value gave a good output response which did not appear to be over compensated.

The harmonic drive actuator used in this experiment has over 215 Nm of torque and operates at a gear reduction ratio of 1:50 [27]. Due to the physical structure of a harmonic drive, the internal flexspline used to rotate the motor output shaft creates a lot of internal friction within the motor, therefore making it a perfect candidate for this friction compensation technique. The internal friction of the gear drive prevents it from being backdrivable. In addition to this, the error signal must have a magnitude of around one radian to drive the motor or else the motor shaft will not rotate.

A decreasing amplitude chirp waveform was selected to be the input used for the GA identification, as was recommended in Section 4.1.1. The details of how the input signal was constructed are outlined in Appendix C. Data was collected at a sampling rate of 0.01 seconds and is shown in Figure 5.5. At the beginning, the harmonic drive was commanded to rotate 177° (3.09 radians) counterclockwise; however the shaft only reached 127.8° (2.231 radians) before the motor shaft began to change direction. As the frequency of the input signal increased, the motor began to respond less and less, until around the 220 second mark when the motor stopped rotating at all.

Signs of the internal friction in the motor are evident by comparing the input and output signals. The output signal lags the input by a few seconds, since the signal sent to the motor needs to be large before the motor will respond. At the lower frequencies, the output signal also appears to be clipped at the extremes. A motor with high internal friction will have poor precision, resulting in what appears to be clipping in the output signal.

The collected input and output data pair was processed through the GA and a friction model was identified whose constant velocity characteristic is shown in Figure 5.6. The GA that was used contained 10 Parents and 8 Children. All the Parents were randomly initialized to have parameter values between 0.01 and 1.5.

The friction model that was identified to be the best *fit* for the particular data pair collected, was the exponential friction model shown in (21). The parameter values which the GA always

converges to are shown in Table 5.2. The *fit* value that the friction model converged to was equal to 86.4.

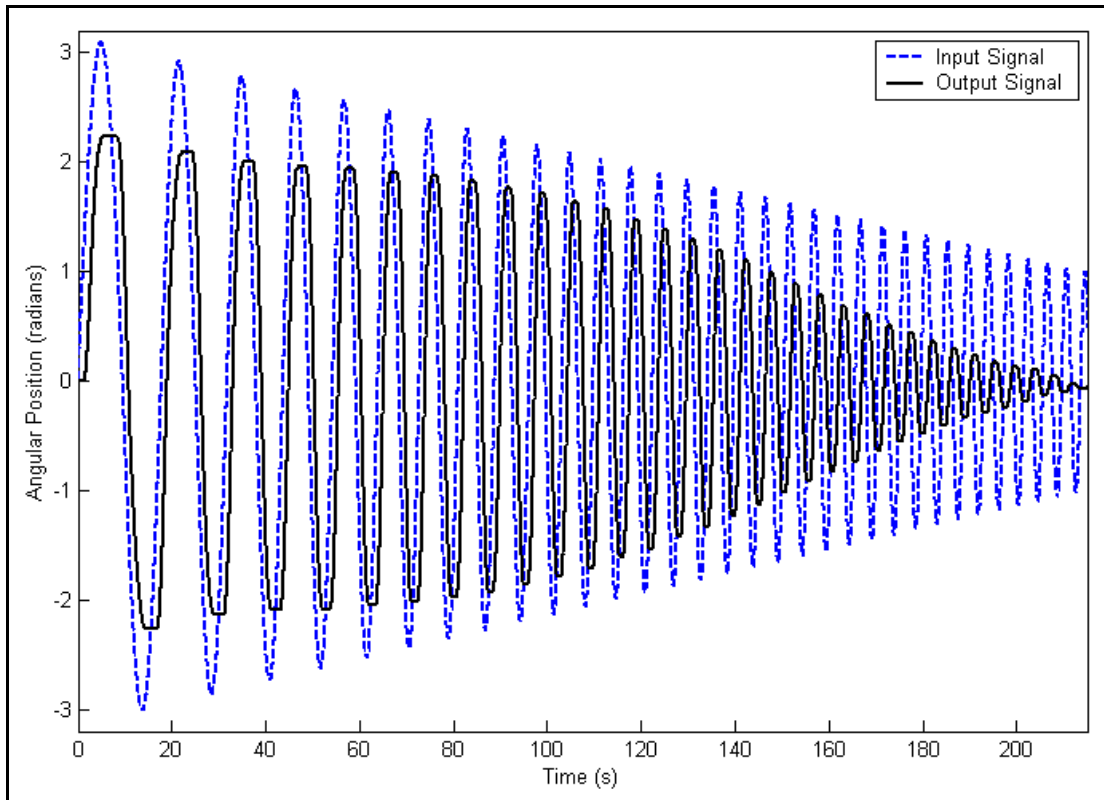


Figure 5.5 Collected Input and Output Data Pair

Table 5.2 Exponential Model Parameterization

F_s	γ	δ	F_c	σ
1.5281	4.3743	0.1992	0.3303	0.0588

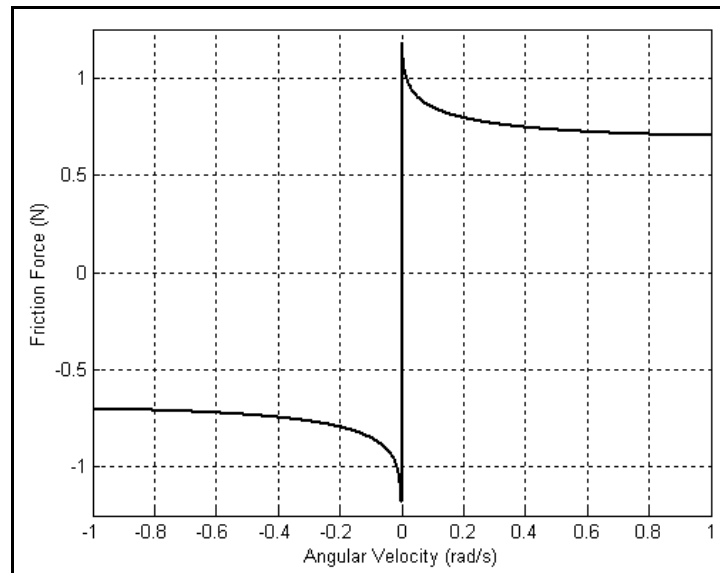


Figure 5.6 Identified Constant Velocity Friction Model

The GA also identified the linear motor model parameters for (20). Their values converge to the results shown in Table 5.3.

Table 5.3 Motor Model Parameterization

J_m	B_m
0.2734	0.2738

The identified exponential friction model was implemented in the feedback configuration shown previously in Figure 5.4. The results from running the harmonic drive with, and without friction compensation are shown in Figure 5.7.

The input signal used for these results was a composition of parabolas to form a continuously differentiable waveform. The time duration and the amplitude of each of the parabolas were varied to excite different dynamics in the harmonic drive. The details of the construction of this input signal are shown in Appendix C.

Three different lines are shown in Figure 5.7. The red dashed line shows how the motor should behave in pure simulation under the assumption that no friction is present. This response is generated by applying the input signal to just the motor model identified by the GA. The black dotted line shows how the harmonic drive behaved under no friction compensation control. The output characteristic lags the simulated results as expected. The blue solid line shows the harmonic drive behavior with friction compensation enabled. Both the blue solid line and the black dotted line were plotted using data collected from the harmonic drive.

It is evident that the friction compensation technique has a dramatic effect on the operation of the harmonic drive. There are only a few locations where the simulated results do not match the harmonic drive output. In these locations, the simulation shows that the motor should oscillate very quickly. However, the harmonic drive cannot react fast enough to follow the simulation.

Further analysis was done using the friction compensator designed by the GA. The experimental setup remained the same; however the input signal was changed to a random step generator. The input was created by randomly generating a value and holding it for 2 seconds before randomly generating another value. The waveform that is created using this technique is non-differentiable at the transition times ($t = 2, 4, 6$ etc).

The results from the second analysis are shown in Figure 5.8. In both of the plots in Figure 5.8 the red dashed line represents how the motor behaved in pure simulation with no friction; the dotted blue line shows what the input to the motor was, and the solid black line shows how the harmonic drive reacted to the input. The black line was plotted using experimental data collected from the harmonic drive.

The plot located at the top of Figure 5.8 shows how the harmonic drive reacted with no friction compensation. Even though the input signal varied quite a bit, the harmonic drive's shaft did not move very much since this input signal was not large enough to overcome static friction.

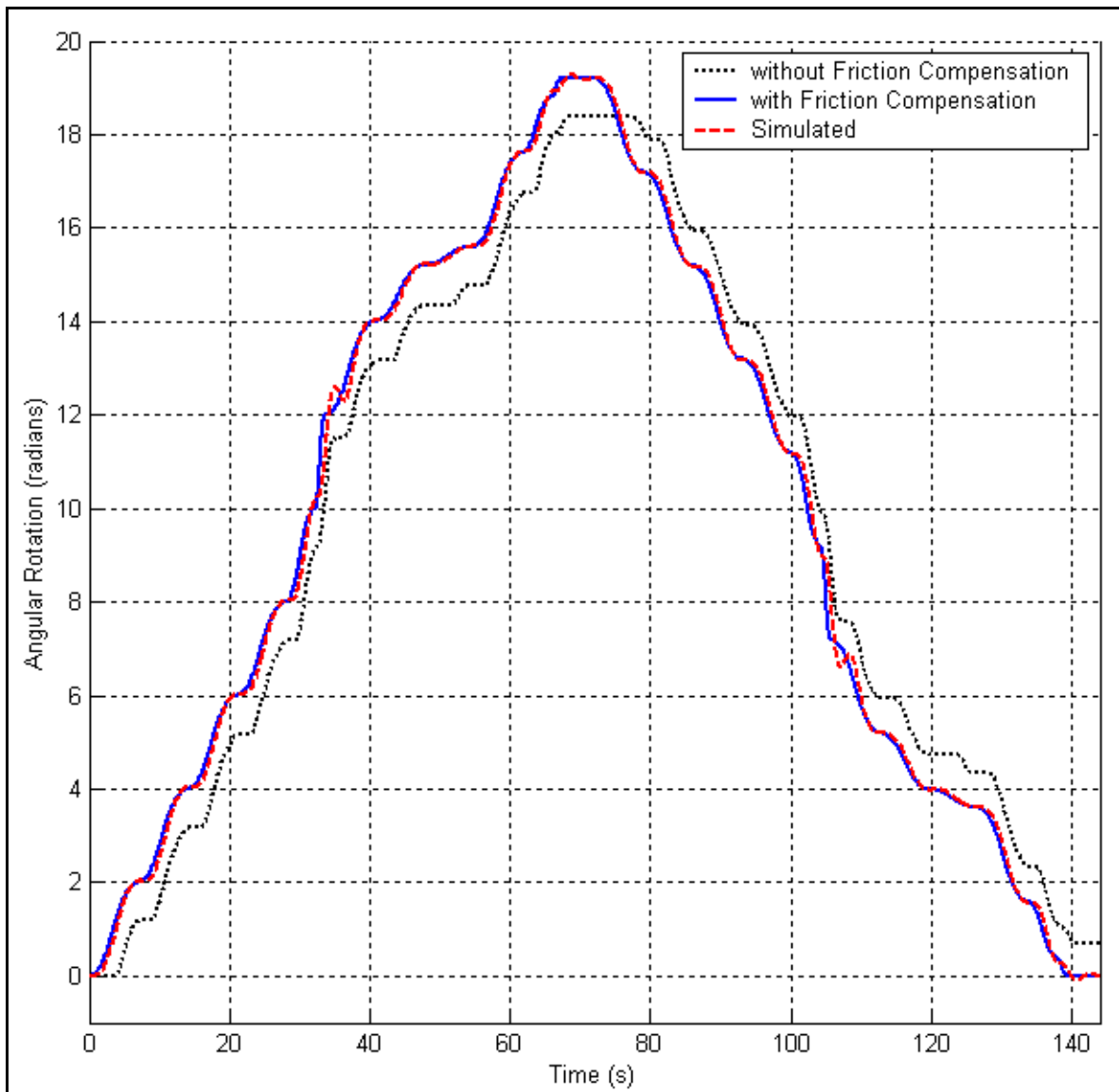


Figure 5.7 Experimental Setup Results

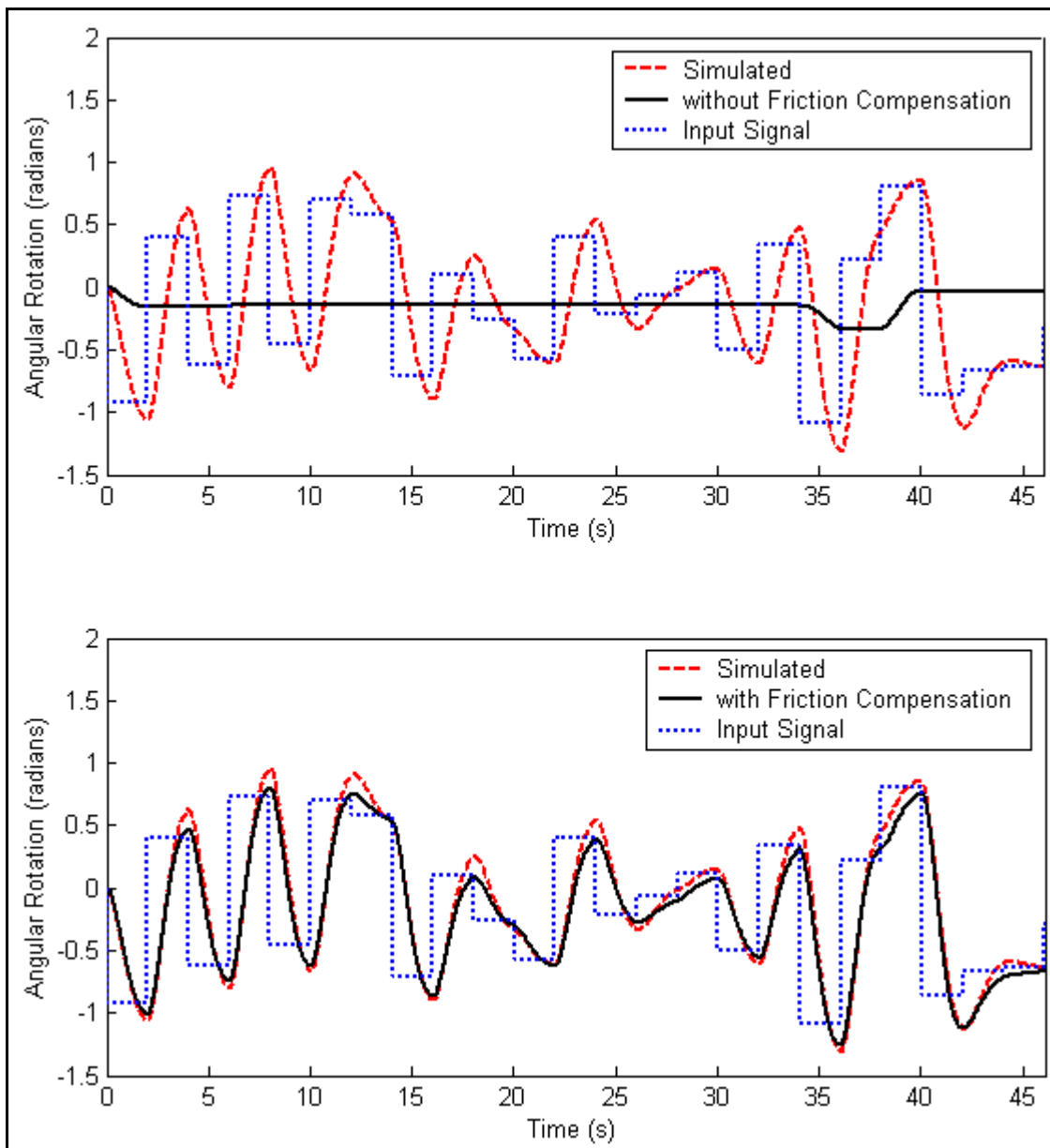


Figure 5.8 Second Experiment Setup Results

The plot located at the bottom of Figure 5.8 shows how the harmonic drive reacted with friction compensation enabled. The same input signal was now able to move the harmonic drive, and the motion matched closely to that of the simulated results. The harmonic drive's output matches more closely to the simulation at all the troughs but not as closely at all the

peaks. This can be explained by friction not being symmetric in both the clockwise and counterclockwise rotation directions. Methods to accommodate this will be discussed in more detail in Chapter 6.

The last experiment performed using the friction compensator was done in open loop. The setup was similar to that shown in Figure 5.4. However, the input was set to zero, and there was no feedback from the output of the motor going back to the input. Under these conditions the output shaft of the harmonic drive was grasped and an attempt was made to turn it by hand. This test was performed to see if the friction compensator could make the motor backdrivable. The results are shown in Figure 5.9.

Initiating motion in the harmonic drive was possible through the use of an external torque. Without the friction compensation, the motor felt very stiff due to its internal friction, thus making it not backdrivable, and it would not move at all. With the friction compensation enabled, it began to rotate slowly with a relatively constant angular velocity after applying a small torque by hand. When a resistive counter torque is applied by hand to the rotating shaft, the harmonic drive comes to a stop. In Figure 5.9, it is evident when the external torque was applied to the motor because the velocity curve formed a spike at that moment. When the rotating shaft was resisted, the velocity of the output shaft went to zero.

The results from this experiment are important because they show that the friction compensator is behaving correctly. According to Newton's first law, if no net force is acting on the motor shaft, then after a brief pulse of external torque, the shaft will continue rotating at a constant velocity [40]. This is the exact result that was observed; therefore the internal friction in the motor must be modeled to a reasonably high degree of accuracy.

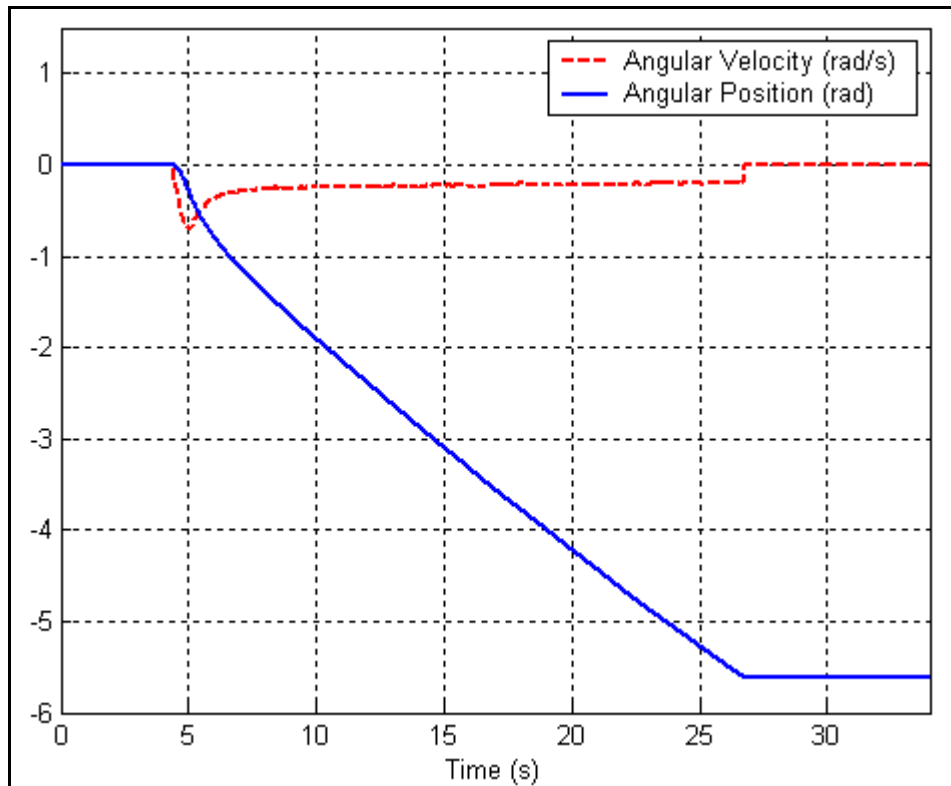


Figure 5.9 Backdrivability Results

5.4 Applied Friction Compensation Summary

This chapter outlined a detailed procedure that could be followed to successfully implement a friction compensation technique using the results gathered from the GA. This friction compensation technique was then used on a harmonic drive to improve its operating performance. Experiments show that the friction compensation does indeed affect the operation of the harmonic drive in a positive manner. The harmonic drive exhibited less internal friction and as a result, could be controlled more accurately than if no friction compensation was used. In addition to this, the friction compensator worked so well that the shaft of the motor could be backdrivable. Some abnormalities were noticed in the friction compensation technique in Figure 5.8, and these will be discussed further in the next chapter.

Chapter 6

Conclusions and Recommendations

In the previous chapters, a method was presented showing how to create a friction compensator for an electric motor. This method uses the optimization capabilities of a Genetic Algorithm to parameterize and rate the effectiveness of different friction models. The unique result found in this thesis is that many different model-based friction compensators can be analyzed and parameterized, for use in a friction compensation technique. Different friction models can be rated according to their capabilities to model the true frictional effects in the system which is being analyzed. A systematic procedure is developed to determine which friction model best characterizes the real friction in a motor. Unique parameterization for all the friction models and motor models are attainable through the use of the GA. Experimental results shown in Chapter 5 prove that this method is effective when deployed on a harmonic drive actuator.

Another great result from using this friction compensation technique is that a non-linear motor with friction can be converted to a linear motor model without friction. Linear control theory can be used on the identified motor model to further improve the performance of the motor under test.

Harmonic drives are known to inherently suffer from internal friction due to their physical construction, thus making them difficult to backdrive. The friction compensator used on the harmonic drive gave exceptional results. The precision of the motor was increased dramatically since most of the internal friction was eliminated and in open loop, the motor was backdrivable.

Future work which could be done to further improve the GA is outlined below. In Chapter 5, after analyzing the experimental data, it was noticed that the friction compensated system did not improve its performance equally in both the clockwise and counterclockwise directions. This is easily explained by the fact that the true friction in the harmonic drive is not symmetrical. That is, the magnitude of the friction which the motor experiences in the

clockwise direction is not the same as the magnitude of the friction which the motor experiences in the counterclockwise direction. In the Genetic Algorithm implementation of each of the friction models, it is assumed that the models are symmetric to reduce the offline computation time for finding the model parameter values. If symmetry is not assumed, then the Genetic Algorithm would have to run at least twice as long. If the motor could be actuated in only one direction at a time during data collection for the GA, then one friction model could be identified for the positive velocities, and another friction model could be identified for the negative velocities. This would require the GA to be run at least two times. The resulting two friction models could be combined to give a non-symmetrical friction model.

If the motor has a restricted range of motion under which it can operate, thus not allowing it to be actuated in only one direction for a period of time long enough to collect a sufficient amount of data, then the GA would need to be modified. The modification would need to generalize the GA's search capabilities so that one set of parameters could be identified during positive velocity motion, and another set of parameters could be identified for negative velocity motion.

Some other recommendations to the Genetic Algorithm are listed below as possible methods of improving the performance of the resulting friction compensator.

In Chapter 2, six models were described as being potential candidates for modeling friction. Since the Genetic Algorithm only finds values for each of the parameters in the models, it is not necessary for the parameters to have a physical representation. With this in mind, it might be possible to find a friction model which fits the collected data by using a very general friction model structure such as a series of connected splines.

Another change that could be made to the Genetic Algorithm that may improve its performance is to allow for the friction model parameter values to take on negative values. Currently the Genetic Algorithm is designed to only use positive values, but by allowing negative values for each of the parameters, a wider range of friction curves could be generated.

Some friction models may be able to model certain physical friction effects better than other models. Therefore, if a few friction models could be combined together internally in the GA, it might be possible to find a better resulting friction model of the true friction. How to combine the different friction models inside the GA would be the difficult part. One possibility is a linear combination of the models.

Lastly, an addition of a Neural Network to this friction compensation technique could improve the overall performance of the technique. The model-based friction compensator can be used to model much of the friction in the system and the un-modeled dynamics such as variations in friction due to temperature and non-symmetry of the friction model, could all be characterized by the Neural Network. This sort of friction compensation has been dubbed Intelligent Friction Compensation, and has proven to be very effective [31].

Industrial robotic applications are an example where this friction compensation technology would be very useful. Industries which require precise motion control such as medical micro surgery robots or robots in automobile assembly plant would benefit from using this technology. The ability to backdrive a harmonic drive allows applications such as tele-robotics to be use these kinds of actuators.

It is common practice in industry to purchase motors which are very expensive to ensure a high degree of precision is attainable. With this friction compensation technology, less expensive motors could be purchased and outfitted with friction compensators to achieve the same high degree of precision as their more expensive counter parts. Since motors are used in a very wide field of applications, this friction compensation technique could result in many industrial relevant applications.

Glossary

This list contains commonly used terms and their definitions, used throughout this thesis.

ADC	Acronym for Analog to Digital Converter
Asperity	A slight projection from a surface on a microscopic level; a point or bump.
Backdrivable	Either the ability or the qualitative degree of ease with which the joint of a robot arm can be forced to move in such a way that all mechanical transmission components, including the motor rotor, can move also.
Backlash	Backlash, or freeplay between input and output of a motor, is typically caused by movement of gear teeth back and forth within tooth spaces, and results in lost motion or error.
Break-Away Force	The force required to overcome the stiction and initiate gross motion.
Children/Child	A GA component that contains a possible solution. Each Child is derived from a Parent.
Coulomb Friction	Friction that is directly proportional to the normal force acting on the object.
DAC	Acronym for Digital to Analog Converter
DAQ	Acronym for Data Acquisition
Dahl Effect	The microscopic relative motion of contacting bodies due to elastic deformation of their asperities.
Dwell Time	The time that the system has spent at zero velocity.
Dynamic Friction	See Viscous Friction.
Evolutionary Algorithm	Probabilistic optimization technique, motivated by the process of natural evolution found in biological organisms.
Friction	A force that resists the relative motion or tendency to such motion of two bodies in contact.
GA	Acronym for Genetic Algorithm.

Genetic Algorithm	A subset of Evolutionary Algorithms which uses a Parent and Child structure.
Harmonic Drive	A harmonic drive is an extremely precise, zero-backlash speed reduction system that operates very differently from conventional toothed gear motors.
Hysteresis	The lagging of an effect behind its cause.
Parent	A GA component that contains a possible solution. A Parent is used to generate new Children during each iteration through the GA.
Pre-Sliding Motion	Motion that occurs at a microscopic level during break-away.
Static Friction	This is the amount of force that is needed to initiate motion.
Stiction	Short for Static Friction. The friction when sticking occurs.
Stribeck Effect	The tendency of the frictional force in lubricated systems to decrease when the velocity of the moving bodies is increased from zero.
Tribology	A study that deals with the design, friction, wear, and lubrication of interacting surfaces in relative motion (as in bearings or gears).
Viscous	Having relatively high resistance to flow.
Viscous Friction	Friction which is directly proportional to the relative velocity of the moving bodies. This type of friction is sometimes referred to as dynamic friction.

Appendix A

Uniform Random Variable Theory

The following information has been collected from [39].

A random variable is said to be uniformly distributed over the interval (α, β) if its probability density function is given by,

$$f(x) = \begin{cases} \frac{1}{\beta - \alpha} & \text{if } \alpha < x < \beta \\ 0 & \text{otherwise} \end{cases} . \quad (28)$$

Since $f(x) > 0$ only when $x \in (\alpha, \beta)$, it follows that X must assume a value in (α, β) . Also since $f(x)$ is constant for $x \in (\alpha, \beta)$, X is just as likely to be near any value in (α, β) as any other value.

The mean or $E[X]$ of a uniform random variable can be calculated to be equal to,

$$\begin{aligned} E[X] &= \int_{-\infty}^{\infty} x \cdot f(x) \cdot dx \\ &= \int_{\alpha}^{\beta} \frac{x}{\beta - \alpha} dx \\ &= \frac{\beta^2 - \alpha^2}{2 \cdot (\beta - \alpha)} \\ &= \frac{\beta + \alpha}{2} . \end{aligned} \quad (29)$$

In other words, the expected value of a random variable uniformly distributed over some interval is equal to the midpoint of the interval.

The variance of a uniform random variable can be calculated as,

$$\text{Var}(X) = E[X^2] - (E[X])^2 \quad (30)$$

Therefore, we first calculate $E[X^2]$,

$$\begin{aligned} E[X^2] &= \int_{\alpha}^{\beta} \frac{1}{\beta - \alpha} x^2 \cdot dx \\ &= \frac{\beta^3 - \alpha^3}{3 \cdot (\beta - \alpha)} \\ &= \frac{\beta^2 + \alpha \cdot \beta + \alpha^2}{3}. \end{aligned} \quad (31)$$

Hence,

$$\begin{aligned} \text{Var}(X) &= \frac{\beta^2 + \alpha \cdot \beta + \alpha^2}{3} - \left(\frac{\beta + \alpha}{2} \right)^2 \\ &= \frac{(\beta - \alpha)^2}{12}. \end{aligned} \quad (32)$$

The standard deviation (σ) is related to the variance, hence we can solve for σ as follows,

$$\begin{aligned} \sigma^2 &= \text{Var}(X) \\ \sigma^2 &= \frac{(\beta - \alpha)^2}{12} \\ \sigma &= \frac{(\beta - \alpha)}{\sqrt{12}}. \end{aligned} \quad (33)$$

Appendix B

Harmonic Drive Construction

The following information was extracted from (41).

A harmonic drive is an extremely precise, zero-backlash speed reduction system that operates very differently from conventional toothed gear forms. A radial, rather than a rotating, tooth mesh is created by flexing one element to create an inward and outward tooth motion, which allows a spline-like tooth engagement. The result is a transmission that delivers precise angular position, in very high input-to-output rotation (50:1 & up), and is light and compact in relation to the large torque that it generates.

Backlash, or freeplay between input and output, is typically caused by movement of gear teeth back and forth within tooth spaces, and results in lost motion or error. In a Harmonic Drive, true backlash is limited to mechanical clearance in the wave generator input coupling and, because of high gear ratios, is almost negligible at the output.

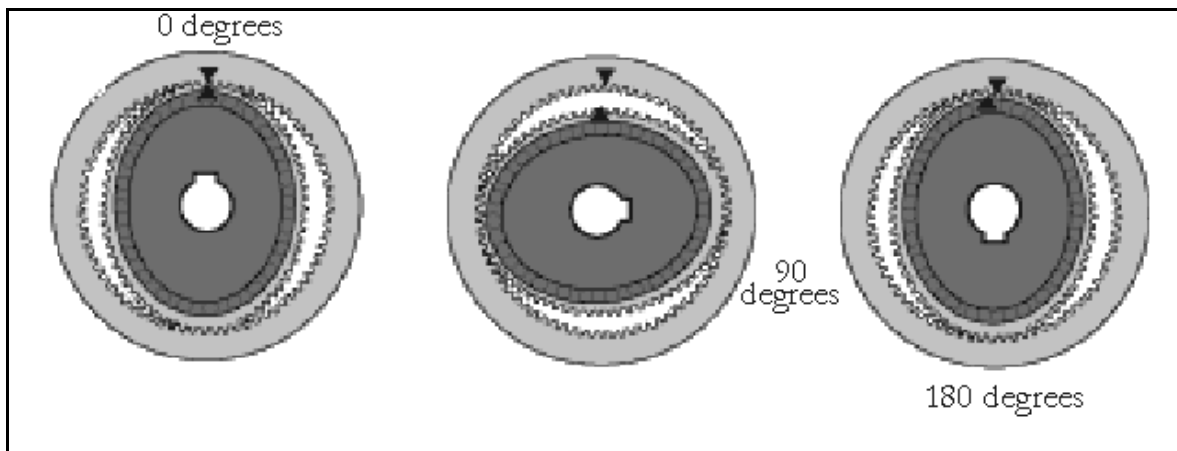


Figure A.1 Harmonic Drive Motion

An elliptical wave generator input deflects the flexspline to engage teeth at the major axis as shown in the first illustration in Figure A.1. Note that the amount of flexspline deflection shown in the figure has been exaggerated in order to demonstrate the principle. Actual deflection is much smaller than shown and is well within the material fatigue limits. Flexspline teeth at minor axis are fully disengaged; most of the relative motion between teeth occurs here.

Flexspline output rotates in the opposite direction to the input. The rigid outer circular spline is rotationally fixed.

The teeth on the non-rigid flexspline and the rigid circular spline are in continuous engagement. Since the flexspline has two teeth fewer than the circular spline, one revolution of the input causes relative motion between the flexspline and the circular spline equal to two teeth. With the circular spline rotationally fixed, the flexspline rotates in the opposite direction to the input at a reduction ratio equal to one-half the number of teeth on the flexspline.

This relative motion may be seen by examining the motion of a single flexspline tooth over one-half an input revolution. The tooth is fully engaged when the major axis of the wave generator input is at 0° . When the wave generator's major axis rotates to 90° , the tooth is fully disengaged. Full reengagement occurs in the adjacent circular spline tooth space when the major axis rotates another 180° back to 0° , thereby producing the two tooth advancement per input revolution.

All tabulated harmonic drive gear reduction ratios assume output through the flexspline with the circular spline rotationally fixed. However, any drive element may function as the input, output, or fixed member.

Appendix C

Experimental Setup Inputs

The following section outlines how to construct the input signals used in the experimental results.

A decreasing amplitude chirp signal (DACS) input was used to collect output data from the harmonic drive to be used in the GA. The chirp signal began its frequency sweep at 0.3 radians/second and increased to 1.5 radians/second over 200 seconds. The amplitude of the chirp signal was attenuated by multiplying the chirp signal by the following function,

$$-0.01 \cdot t + \pi. \quad (34)$$

In (34), t represents the time in seconds.

To confirm that the friction compensation technique works properly, a composition of parabolas was used as an input signal. This signal is comprised of the following curve joined end to end to form a continuously differentiable function.

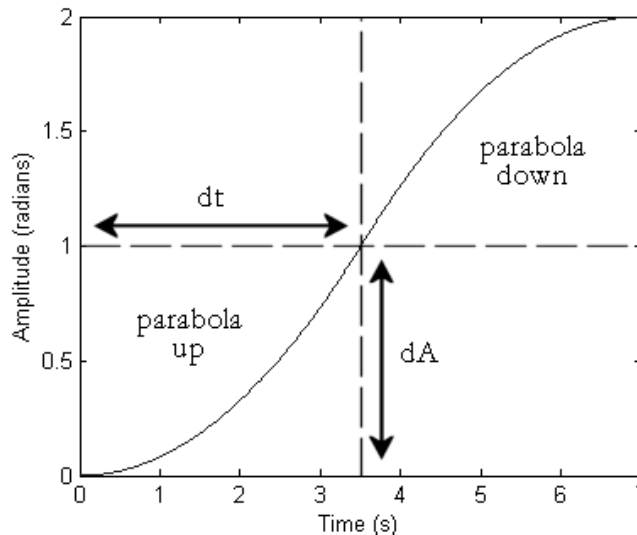


Figure C.1 Parabola Up and Down

Tabx below summarizes how the input signal was created. Each section is made up of one parabola facing up and one parabola facing down.

Table C.1 Input Signal Break-down

Section	dt	dA	ends at t =	ends at A =
1	3.5	1.0	7	2
2	3.5	1.0	14	4
3	3.5	1.0	21	6
4	3.5	1.0	28	8
5	2.1	1.0	32.2	10
6	0.7	1.0	33.6	12
7	3.5	1.0	40.6	14
8	3.5	0.6	47.6	15.2
9	3.5	0.2	54.6	15.6
10	3.5	1	61.6	17.6
11	2.1	0.6	65.8	18.8
12	0.7	0.2	67.2	19.2
13	0	0	72	19.2
14	3.5	-1	79	17.2
15	3.5	-1	86	15.2
16	3.5	-1	93	13.2
17	3.5	-1	100	11.2
18	2.1	-1	104.2	9.2
19	0.7	-1	105.6	7.2
20	3.5	-1	112.6	5.2
21	3.5	-0.6	119.6	4
22	3.5	-0.2	126.6	3.6
23	3.5	-1	133.6	1.6
24	2.1	-0.6	137.8	0.4
25	0.7	-0.2	139.2	0
26	0	0	141	0

Bibliography

- [1] F.P.Bowden and D. Tabor. Friction - An Introduction to Tribology, Anchor Books, 1973.
- [2] F.P. Bowden, Frank Philip. Friction; An Introduction to Tribology, 1973.
- [3] F.P. Bowden and D. Tabor. The Friction and Lubrication of Solids, Oxford University Press, Oxford, 1950.
- [4] F.P. Bowden and D. Tabor. The Friction of Lubrication of Solids, Part II, Oxford University Press, Oxford, 1964.
- [5] H. Olsson, K.J. Astrom, C. Canudas de Wit, M. Gafvert, P. Lischinsky. Friction Models and Friction Compensation, 1997.
- [6] R. Stribeck. Die wesentlichen Eigenschaften der Gleit-und Rollenlager – The key qualities of sliding and roller bearings. Zeitschrift des Vereines Seutscher Ingenieure, 46(38,39):1342-48,1432-37, 1902.
- [7] B. Armstrong-Helouvry, P. Dupont and C. Canudas de Wit. A Survey of Models, Analysis Tools and Compensation Methods for the Control of Machines with Friction, Automatica, Vol 30 No 7, 1083-1138, 1994.
- [8] Ernest Rabinowicz. The nature of the static and kinetic coefficients of friction. Journal of Applied Physics, 22(11):1373-79, 1951.
- [9] V.I. Johannes, M.A. Green and C.A. Brockley. The role of the rate of application of the tangential force in determining the static friction coefficient, Wear, 24:381-385, 1973.
- [10] B. Armstrong-Helouvry. Control of Machines with Friction, Kluwer Academic Publishers, 1991.
- [11] B. Friedland and Y.J. Park. On adaptive friction compensation. In Proceedings of the IEEE Conference on Decision and Control, pg 2899-2902, 1991.

- [12] C.B. Baril. Control of Mechanical Systems Affected by Friction and Other Nondifferentiable Nonlinearities. PhD thesis, Technion, Israel Institute of Technology, Haifa, Israel, 1993.
- [13] O. Reynolds. On the theory of lubrication and its application to Mr. Beauchamp Tower's experiments, including an experimental determination of the viscosity of olive oil. Phil. Trans. Royal Soc., 177:157-234, 1886.
- [14] A.J. Morin. New friction experiments carried out at Metz in 1831-1833. In Proceedings of the French Royal Academy of Sciences, volume 4, pg 1-128. 1833.
- [15] P.A. Bliman and M. Sorine. Easy to use realistic dry friction modes for automatic control. In Proceedings of 3rd European Control Conference, Rome, Italy, pg 3788-3794, 1995.
- [16] L. Bo and D. Pavelescu. The Friction-Speed relation and its Influence on the Critical Velocity of Stick-Slip Motion, Wear, Vol 82, pg 277, 1982.
- [17] A. Tustin. The Effects of Backlash and Speed-Dependent Friction on the Stability of Closed Cycle Control System, Journal of IEEE, Vol. 94, pp 143-151, 1947.
- [18] C. Canudas de Wit, P.Noel, A. Aubin and B. Brogliato. Adaptive Friction Compensation in Robot Manipulators: Low Velocities. International Journal of Robotics Research, Vol 10 No. 3, pp189-199, 1991.
- [19] Pierre E. Dupont. Avoiding Stick-Slip Through PD Control. IEEE Transactions on Automatic Control Vol 39, No 5, May 1994.
- [20] C.Canudas de Wit, H. Olsson, K.J. Astrom, and P. Lischinsky. A New Model for Control of Systems with Friction. IEEE Transactions on Automatic Control, Vol 40, No 3, pp 419-425, March 1995.
- [21] B. Armstrong. Friction: Experimental Determination, Modeling and Compensation. Proceedings of the IEEE Conference on Robotics and Automation, pp 1422-1427, 1988.

- [22] H.P. Schwefel. Numerical Optimization of Computer Models, John Wiley, Chichester, UK, 1981.
- [23] L.J. Fogel, A. J. Owens, and M. J. Walsh. Artificial Intelligence through Simulated Evolution. John Wiley, New York, 1966.
- [24] J.H. Holland. Adaptation in Natural and Artificial Systems. University of Michigan Press, Ann Arbor, 1975.
- [25] S.S. Rao. Optimization: Theory and Applications. Wiley Eastern, New Delhi, 1984.
- [26] Sheldon Ross. A First Course in Probability Fifth Edition. Prentice-Hall, NJ, 1998.
- [27] Harmonic Drive Data Sheet is located at the following URL (visited November 2002). http://hdsi.net/Product/data/RFS_actuators/loader.cfm?format=metric&RFS=32-6030
- [28] P.E. Dupont and E.P. Dunlap. Friction modeling and PD Compensation at Very Low Velocities. Transaction of the ASME, Vol 117, pp8-14, March 1995.
- [29] C. Ganseman, J. Swevers and F. Al-Bender. An Integrated Friction Model with Improved Pre-Sliding Behavior. 1997.
- [30] URL (visited December 2002). <http://www.mdrobotics.ca>
- [31] Wenfang Xie, Marek Krzeminski, David Wang, Hussein El-Tahan, Mona El-Tahan, Intelligent Friction Compensation (IFC) in a Harmonic Drive, Presented at the Newfoundland Electrical and Computer Engineering Conference (NECEC 2002), St. John's, Newfoundland, Nov. 2002.
- [32] R.S.H. Richardson and H. Nolle. Surface Friction Under Time-Dependent Loads. Wear 37(1): 87-101, 1976.

- [33] J. Courtney Pratt and E. Eisner. The Effect of a Tangential Force on the Contact of Metallic Bodies. In Proceedings of the Royal Society. Vol A238, pg 529-550, 1957.
- [34] Kevin Tuer. Development of Intelligent Friction Compensation (IFC) Techniques, Literature Survey. CSA Contract #9F028-004102\012\MTC, 2001.
- [35] Z. Michalewicz. Genetic Algorithms + Data Structures = Evolution Programs. Springer-Verlag, New York, 1996.
- [36] L.J. Eshelman, R.A. Caruana, and J. D. Schaffer. Biases in the Crossover Landscape, Proceedings of the 3rd International Conference on Genetic Algorithms, 1989, pp. 10-19.
- [37] Z. Michalewicz and C. Janikow. Genetic Algorithms for Numerical Optimization, Statistics and Computing, vol. 1, no. 1, 1991.
- [38] Richard C. Dorf, Robert H. Bishop. Modern Control Systems 8th Edition, Addison Wesley, pg 182-183, 1998.
- [39] Sheldon Ross. A First Course in Probability 5th Edition. Prentice Hall, New Jersey, 1998.
- [40] David Halliday, Robert Resnick, Jearl Walker. Fundamentals of Physics extended with Modern Physics, 4th Edition. John Wiley & Sons Inc. pg 98, 1993.
- [41] URL (visited December 2002). <http://www.harmonic-drive.com>
- [42] Thambirajah Ravichandran, PhD Thesis in progress, University of Waterloo, 2002.